The Lower Limb and Mechanics of Walking in *Australopithecus sediba*

Jeremy M. DeSilva,[1,2]* Kenneth G. Holt,[3] Steven E. Churchill,[4,2] Kristian J. Carlson,[2,5] Christopher S. Walker,[4] Bernhard Zipfel,[2,6] Lee R. Berger[2]

The discovery of a relatively complete *Australopithecus sediba* adult female skeleton permits a detailed locomotor analysis in which joint systems can be integrated to form a comprehensive picture of gait kinematics in this late australopith. Here we describe the lower limb anatomy of *Au. sediba* and hypothesize that this species walked with a fully extended leg and with an inverted foot during the swing phase of bipedal walking. Initial contact of the lateral foot with the ground resulted in a large pronatory torque around the joints of the foot that caused extreme medial weight transfer (hyperpronation) into the toe-off phase of the gait cycle (late pronation). These bipedal mechanics are different from those often reconstructed for other australopiths and suggest that there may have been several forms of bipedalism during the Plio-Pleistocene.

The locality of Malapa, South Africa, has yielded two relatively complete skeletons of *Australopithecus sediba*, dated at 1.977 million years ago (*1*, *2*). This species has a combination of primitive and derived features in the hand (*3*), upper limb (*4*), thorax (*5*), spine (*6*), and foot (*7*) in a hominin with a relatively small brain (*8*), a human-like pelvis (*9*), and a mosaic of *Homo*- and *Australopithecus*-like craniodental anatomy (*1*, *10*, *11*). The foot in particular possesses an anatomical mosaic not present in either *Au. afarensis* or *Au. africanus* (*7*), supporting the contention that there were multiple forms of bipedal locomotion in the Plio-Pleistocene (*12*). The recent discovery of an *Ardipithecus*-like foot from 3.4-million-year-old deposits at Burtele, Ethiopia, further shows that at least two different kinematic solutions to bipedalism coexisted in the Pliocene (*13*). Here we describe the lower limb of *Au. sediba* [specimen numbers and attributions are provided in table S1 (*14*)] and propose a hypothesis for how this late australopith walked.

Lower Limb of MH1

The holotype of *Au. sediba* is Malapa Hominin 1 (MH1), a juvenile male partial skeleton whose lower limb consists of a right proximal femur (fig. S1), small shaft fragments from the tibia and fibula, and foot bones already described (*7*) (table S1). The proximal femur is australopith-like, with a long, anteroposteriorly compressed femoral neck (fig. S2) and low neck-shaft angle (110° to 115°) (table S2). Posterolaterally, there is a third trochanter, inferior to which is a well-developed hypotrochanteric fossa, a human feature reflecting a large insertion area for the gluteus maximus (*15*).

Lower Limb of MH2

The lower limb of MH2, an adult female, consists of a right femoral head and neck, part of the proximal femoral shaft, the left proximal fibula, and the right knee joint (including the patella). Additionally, as already described (*7*), MH2 preserves an articulated distal tibia, talus, and calcaneus and a partial fifth metatarsal. The proximal femur preserves much of the head and neck (fig. S1). As in MH1, the neck is anteroposteriorly compressed (table S2). Viewed superiorly, the head appears to be prolonged anteriorly, as is the case in most humans (*16*).

The right knee of MH2 is represented by an 86.7-mm-long fragment of the distal femur (fig. S3), two fragments that conjoin to form most of the tibial plateau (fig. S4), and a relatively complete patella composed of two conjoining fragments, one of which remains partially embedded in calcified sediment. This part of the patella has been digitally extracted from micro–computed tomography (μCT) scans, and a nearly complete knee cap has been reconstructed (fig. S5). The posteromedial part of the distal femur has been sheared away, but the lateral condyle, patellar articular surface, distal shaft, and most of the medial condyle are well preserved. The bicondylar angle is estimated to be ~9°, which is within the range of modern humans but is low for an australopith (table S3). There is a sustrochlear hollow just superior to the patellar surface, evidence of contact with the patella in a fully extended position (*17*) (fig. S6). There is a strong medial condylar boss, an anatomy unique to hominins, and evidence for a "tibial dominant" knee capable of full extension (*18*) (fig. S7). Most notable is the high lateral patellar lip. The lateral trochlear groove angle (*19*) is 31.3°, 3 SD above the modern human mean (*20*) and far greater than any ape trochlear angle, because apes tend to have flat trochlear grooves (Fig. 1). A high lateral patellar lip serves as a bony mechanism for patellar retention during bipedal gait (*21*, *22*). The extension of the lateral lip in *Au. sediba* is not a function of overall anterior expansion of the patellar surface, as is found in *Homo* (*18*), and is restricted just to the lateral side (fig. S8). Laterally, there is a deep groove for the popliteus, an internal rotator of the tibia and stabilizer of the knee. This muscle may have been important in resisting internal rotation of the femur during stance phase. The relatively narrow tibial spines on the MH2 tibial plateau suggest enhanced knee mobility (*23*), although this anatomy may also be related to the small size of *Au. sediba* (*24*).

On the proximal tibia, the medial condyle is flat and the lateral condyle is slightly convex anteroposteriorly, similar to the condition found in other small australopiths (specimens A.L. 129-1 and StW 514), although the functional importance of this convexity is unclear (*25*). There appears to be a small notch on the lateral plateau, perhaps indicating the presence of a double meniscus attachment and thus possibly greater osteoligamentous

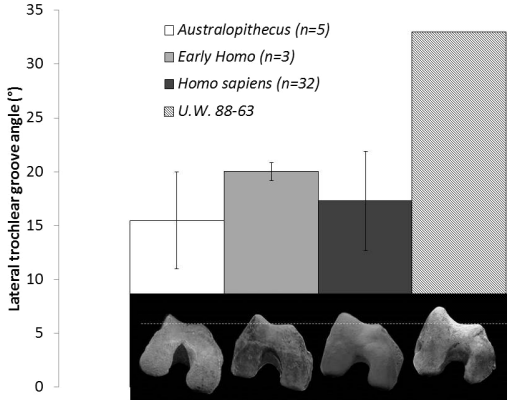

Fig. 1. The lateral patellar lip. The lateral trochlear groove angle (*19*) is similar in *Australopithecus* (TM 1513, Sts 34, A.L. 129-1, A.L. 333-4, and A.L. 333w-56), early *Homo* (KNM-ER 1472, KNM-ER 1481, and KNM-WT 15000), and modern humans (*20*). This measurement in MH2 (U.W. 88-63) is over 3 SD higher than in modern humans. Apes have flat trochlear grooves (*18*) (fig. S7) and thus lateral trochlear groove angles near zero. Bottom images, from left to right, are as follows: TM 1513, KNM-ER 1472, modern human, and MH2, all scaled to the same size. They have been positioned so that the medial patellar surface is horizontal, which corresponds closely to the orientation recommended in (*18*). Note the extreme lateral patellar lip in MH2.

[1]Department of Anthropology, Boston University, 232 Bay State Road, Boston, MA 02215, USA. [2]Evolutionary Studies Institute, University of the Witwatersrand, Private Bag 3, Wits 2050, South Africa. [3]Department of Physical Therapy and Athletic Training, Sargent College, 635 Commonwealth Avenue, Boston University, Boston, MA 02215, USA. [4]Department of Evolutionary Anthropology, Box 90383, Duke University, Durham, NC 27708, USA. [5]Department of Anthropology, Indiana University, Bloomington, IN 47405, USA. [6]Bernard Price Institute for Palaeontological Research, School of Geosciences, University of the Witwatersrand, Private Bag 3, Wits 2050, South Africa.

*Corresponding author. E-mail: jdesilva@bu.edu

control over rotation at the knee as in *Homo* proximal tibiae (*26*). However, the absence of this notch in other australopiths does not necessarily imply the absence of a double insertion (*27*).

The patella is small, measuring 27.1 mm wide mediolaterally and 13.1 mm thick anteroposteriorly. It is 24.7 mm tall superoinferiorly, which is probably just short of the actual height, because there is some damage to the distolateral aspect of the apex. The posterior part of the patella is human-like in being strongly convex mediolaterally (fig. S9), with a high central keel separating the condylar facets medially and laterally.

The most proximal 97.1 mm of the left fibula of MH2 is preserved as four conjoining fragments (fig. S10). The fibula is more gracile than modern ape fibulae and in this respect resembles specimen OH 35 (fig. S11). The MH2 fibula has an osteophytic growth at the biceps femoris insertion.

Lower Limb of MH4

MH4, an adult or near-adult individual of unknown sex, is represented by two conjoining pieces of a tibia described previously (*7*). Here we provide an estimated total length, possible because the proximal tibia, though not recovered, has left a natural cast of its anterior surface in the calcified sediment (fig. S12). We estimate total tibial length at approximately 271 mm, with a possible range of 267 to 275 mm, depending on the degree of proximal tibial retroversion and the proximal projection of the tibial spines.

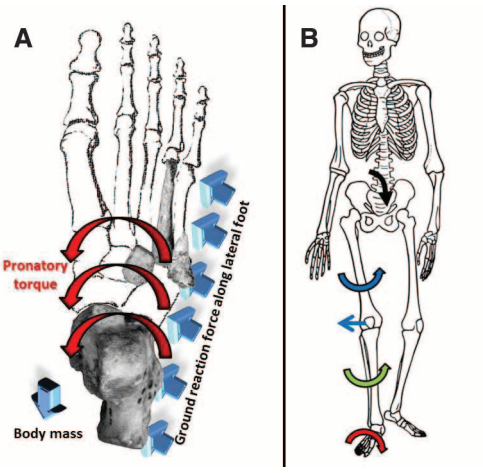

Fig. 2. Hyperpronation. (**A**) The pedal bones of *Au. sediba* are superimposed on a human foot in dorsal view. These bones are not all from the same individual (see table S1 for details). We hypothesize that MH2 would have contacted the ground along the lateral edge of an inverted foot. This would generate a ground reaction resultant (blue arrows) that would be positioned lateral to the joints of the foot, creating a large pronatory torque (red arrows). Although apes often land along the lateral edge of an inverted foot (*30*, *31*), they swing their body mass laterally over the stance foot during bipedal gait, effectively producing a counteracting supinatory torque. *Au. sediba* had a pelvis with sagitally oriented ilia (*9*), suggesting a human-like abductor mechanism and in turn suggesting a medially positioned center of mass relative to the stance leg (illustrated by the large blue arrow at bottom left). This position of the center of mass would exacerbate the pronatory torque at the subtalar, midtarsal, and tarsometatarsal joints. (**B**) Excessive pronation on a weight-bearing foot (curved red arrow) causes a chain of rotatory movements proximal to the foot. The tibia internally rotates (green arrow) as the talus plantarflexes and adducts. The femur also internally rotates [(*42*, *43*); curved blue arrow], increasing the lateral deviation of the patella (small blue arrow). Pronation at the foot causes an anterior pitch of the center of mass [(*34*, *43*); black arrow], counteracted by hyperlordosis of the lumbar region (*6*). *Au. sediba* possesses anatomies that are adaptive to, or consequences of, these motions.

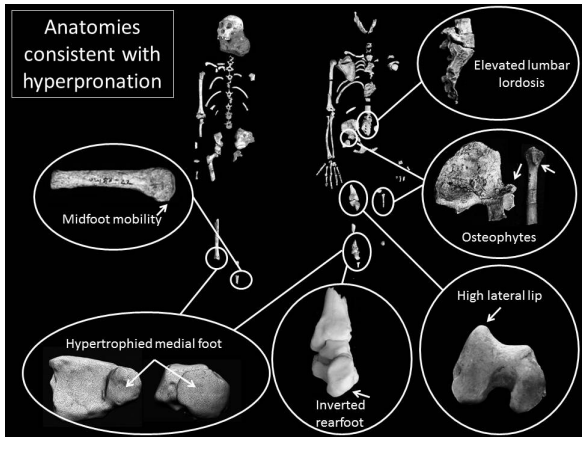

Fig. 3. Skeletons of *Au. sediba*: left, MH1 (pictured with MH4 tibia); right, MH2. Several anatomies of these skeletons are consistent with a hyperpronating gait. The base of the fourth metatarsal is convex, indicating that the midfoot was hypermobile. The medial malleolus and talar head are hypertrophied, reflecting loading of an inverted foot and mobility at the talonavicular joint, respectively. The rearfoot is in an inverted position, a risk factor for hyperpronation in modern humans. Hyperpronators internally rotate the femur and tibia and are at a greater risk for patellar dislocation. The high lateral patellar lip reduces the risk of patellar subluxation. Osteophytes on the origin of the rectus femoris/iliofemoral ligament proximal attachment and insertion of the biceps femoris indicate soft tissue strain: possible consequences of a hyperpronating gait. MH2 has elevated lumbar lordosis (*6*), perhaps to compensate for the excessive anterior pitch of the center of mass common in hyperpronators.

The Kinematics of Walking in *Au. sediba*

The anatomy of the foot (*7*), spine (*6*), pelvis (*9*), and knee (this paper) indicate that *Au. sediba* was an obligate biped. Based primarily on the lower limb, pelvic, and vertebral morphology of MH2, and to a lesser extent on the pedal morphology of MH1, we propose that *Au. sediba* was a hyperpronator (*28*) with exaggerated medial weight transfer during the stance phase of terrestrial bipedalism (Fig. 2). Modern human hyperpronators serve as a kinematic reference model for this gait and its musculoskeletal consequences. We suggest that MH2 expressed this kinematic variation, and *Au. sediba* did with regular frequency, although the hypothesis that the entire species walked in this manner will require further testing with additional fossil material (*14*).

At heel strike of bipedal locomotion, humans commonly have a slightly supinated rearfoot and forefoot, which are passively driven by the ground reaction force into pronation of the subtalar and more distal joints during the subsequent midstance phase of walking. Video and plantar pressure data reveal that apes contact the ground with the heel (*29*) and often the lateral midfoot simultaneously in what has been termed "inverted heel-strike plantigrady" (*30*, *31*). The abducted hallux serves a stabilizing role during quadrupedal walking in apes, contributing little to propulsion (*31*). The divergent hallux is suggested to have served a similar stabilizing role during bipedal walking in *Ardipithecus ramidus* (*32*).

In a small percentage of modern humans, the foot is excessively inverted (termed forefoot and/or rearfoot varus) during the swing phase of walking, resulting in heel strike with the foot in a highly supinated posture, with ground contact established along the lateral border of the heel and forefoot (*33*). Contact between the ground and the lateral side of the foot introduces a large pronatory torque around the subtalar and more distal joints, which drives the foot into pronation (*33*, *34*). As the foot is driven into pronation, there are high medially directed torques that can not only cause excess loading on the bones of the medial column of the foot (*35*) but also stress the soft tissues, such as the ligaments supporting the medial longitudinal arch and the muscles whose tendons insert plantomedially, particularly the tibialis anterior and tibialis posterior. Plantar fasciitis, medial tibial stress syndrome (shin splints), and tibial stress fractures are therefore common injuries experienced by late and hyperpronating modern humans (*34*). Although hyperpronation can have pathological consequences in modern humans, we are proposing here that the skeleton of *Au. sediba* reveals a suite of anatomies that are adaptive for, or consequences of, this kind of walking (Fig. 3).

Reconstruction of the conjoined elements of the rearfoot of MH2 demonstrates that the calcaneus had an inverted set (fig. S13), which is a contributing factor to hyperpronation in modern humans (*36*). However, the inverted heel itself

would not necessarily produce a pronatory torque, because there is considerable variation in the position of the subtalar joint axis relative to the ground reaction force location (*37*). MH2 also had a gracile calcaneal tuber (*7*), with a superiorly positioned lateral plantar process, which reduced the surface area of the plantar aspect of the heel in *Au. sediba* and would have reduced the effectiveness of the subcalcaneal heel pad (based on size information rather than material properties), which has been shown to dissipate peak stress during heel strike (*38*). To compensate, we hypothesize that *Au. sediba* landed simultaneously on the heel and along the lateral foot at touch down, in much the same way that African apes walk (inverted heel-strike plantigrady) (*31*). This is achievable in a bipedal hominin that has full knee extension by slightly increasing normal plantarflexion angle during foot contact. Because of the wider midfoot and forefoot, landing along the lateral side of an inverted foot would provide a large moment arm around the midtarsal and tarsometatarsal joints that would also transfer to the subtalar joint. Thus, a large pronatory torque would drive the foot into pronation (Fig. 2). There is suggestive evidence for excessive pronation in the *Au. sediba* tarsals. An elevated degree of pronation is possible in *Au. sediba*, because the subtalar joint has a high radius of curvature and is therefore quite mobile and capable of an extreme range of motion (*7*). The relatively large talar head of MH2 (*7*) may signal elevated talonavicular mobility, especially because this joint is central to midfoot pronation in humans (*39*).

Landing on an inverted foot would also load the medial portion of the tibiotalar joint and introduce a shear force across the medial malleolus. This may explain the form of the medial malleoli of both MH2 and MH4, which are mediolaterally thicker than those of other fossil hominins or modern humans (*7*). However, pronation does not occur at the tibiotalar joint but at the subtalar joint and joints of the midfoot. As the foot is driven into pronation by a high pronatory torque, the more distal parts of the medial foot would be excessively loaded (*35*). A foot adapted for this kind of locomotion may therefore be expected to exhibit increased mechanical reinforcement of bones in the medial portion of the foot. We predict that, if additional foot elements are recovered, we will see greater joint and diaphyseal robusticity in medial relative to lateral tarsals, metatarsals, and phalanges (Table 1).

Table 1. Evidence for hyperpronation in *Au. sediba*.

Hyperpronating biomechanics	Anatomical predictions	Morphology in *Au. sediba*
Initial ground contact on an inverted foot, resulting in high medially directed forces on tibiotalar joint	Inverted calcaneus and thick medial malleolus	Calcaneus in inverted set and predicted forefoot in varus set; thickest medial malleoli of any known hominin.
Excessive pronation at subtalar joint	Increased mobility at subtalar joint	High radius of curvature of talar facet on calcaneus.
Excessive pronation at midtarsal joints and tarsometatarsal joints	Mobile midfoot in coronal plane	Greatly enlarged talar head, suggestive of talonavicular mobility.
Increased strain on soft tissue of medial foot	Components of medial arch, plantar aponeurosis (if present), and tibialis posterior tendon under stress	Currently unknown. Predicted robust navicular tuberosity; reduced metatarsophalangeal joint extension if plantar aponeurosis taut.
Increased strain on foot bones distally and medially	Increased robusticity of medial tarsals, metatarsals, and phalanges	Currently unknown. Predicted to be relatively robust medially; if partially divergent, hallux could also help counter pronatory torque.
Lowered arch and increased midfoot mobility	Increased sagittal plane dorsiflexion evident in bones of midfoot	Convex surface to base of fourth metatarsal indicative of midtarsal break; predicted concavity of metatarsal facets on cuboid.
Increased knee mobility	Greater rotatory capacity and greater role for knee stabilizers, such as popliteus and biceps femoris	Tibial spines close together and enlarged popliteal groove on distal femur.
Increased internal rotation of femur	Increased strain on muscles crossing both hip and knee joints	Osteophytic growths on both origin for rectus femoris and insertion of biceps femoris. Predicted to have enlarged origin on the anterior superior iliac spine for sartorius.
Increased risk of patellar subluxation	Bony adaptations for patellar retention	Highest lateral patellar lip of any known hominin.
Anterior tilt of the pelvis	Increased lumbar lordosis	Last lumbar vertebra has very high wedging angle.

During midstance, the foot is more mobile and better able to conform to its substrate. In hyperpronators, the talus adducts and plantarflexes excessively, dropping the longitudinal arch and contributing to hypermobility of the midfoot. Although we hypothesize that *Au. sediba* possessed an arched foot (*7*) (fig. S14), there is also evidence for midfoot mobility. A right fourth metatarsal, possibly from MH1, has a highly convex base dorsoplantarly, suggesting the presence of midfoot flexion or a "midtarsal break" (*40*). Other hominin fourth metatarsal bases from *Au. afarensis*, *Au. africanus*, and the OH 8 foot are human-like and do not exhibit evidence for a midtarsal break (Fig. 4) (*40*, *41*). The convexity of the Malapa fourth metatarsal is thus unexpected and implies more mobility at the lateral tarsometatarsal joint in this hominin than in any other. We suggest that the seemingly contradictory anatomies in the foot of *Au. sediba* (possession of an arched foot and long plantar ligament together with midfoot mobility) can only be explained in the context of a bipedal foot that hyperpronates when weight-bearing (*14*).

In modern humans, excessive pronation may have damaging effects in lower limb joints proximal to the foot. In hyperpronators, the tibia and femur both internally rotate excessively (*42*, *43*) under a patella that is relatively fixed by the rectus femoris attachment to the anterior inferior iliac spine (AIIS) as the quadriceps femoris contracts to extend the leg during toe-off (*34*). Because this occurs late in the gait cycle, during knee extension, the patella is pulled laterally, and thus hyperpronators are at risk for both patellofemoral pain (*44*) and patellar subluxation (*45*, *46*). A hominin bony adaptation that helps prevent patellar subluxation is a raised lateral lip of the distal femur (*21*, *22*). The extreme lateral patellar lipping of MH2 (Fig. 1) (figs. S7 and S8) may be an adaptation to resist injurious lateral translation of the patella during hyperpronation of the foot and resulting internal rotation of the tibia and femur during late stance phase. This skeletal adaptation in *Au. sediba* may also implicate a reduced or absent vastus medialis obliquus in counteracting lateral translation of the patella. The fact that a lateral lip is present at birth (*17*, *18*) can be extrapolated to indicate that the species *Au. sediba* (and not just MH2) was adapted for this kind of locomotion (*14*). Furthermore, the large popliteal groove present on the MH2 femur may indicate strong muscular involvement in counteracting the internal rotation of the femur on a fixed tibia, because the popliteus acts as an external rotator of the femur during stance phase.

Hyperpronation drives the entire leg medially during stance phase and may strain any muscle

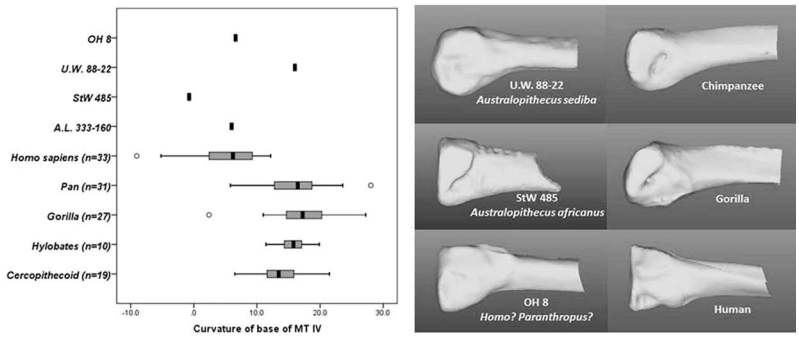

Fig. 4. The fourth metatarsal. (**Left**) Curvature of the base of the fourth metatarsal in fossil hominins, humans, apes, and monkeys (*40*). Humans and most fossil hominins, including *Au. afarensis* (*41*), have flat bases, consistent with a stiff and immobile midfoot. The *Au. sediba* fourth metatarsal has a convex base. [The box-and-whiskers plot shows the median (vertical line), upper and lower quartiles (box), range (whiskers), and outliers (circles) for each group.] (**Right**) Digital renderings of the fourth metatarsal in medial view, illustrating the dorsoplantarly curved base morphology in apes and *Au. sediba* and the flat base in other hominins and in modern humans.

crossing both the knee and the hip joints (e.g., the rectus femoris), particularly those inserting laterally in the leg (e.g., the long head of the biceps femoris). As previously mentioned, the insertion for the biceps femoris on the proximal fibula is osteophytic, indicative of elevated strain on this insertion area (fig. S10). The MH2 ilium has an unusually large and projecting AIIS (fig. S15), suggesting that the rectus femoris (and/or iliofemoral ligament) was under considerable strain during gait. As the femur internally rotates and adducts, the AIIS will be stressed by excessive stretching of the rectus femoris tendinous origin. Finally, hyperpronators experience an anterior pitch of the center of mass relative to the hip joint (*43*), requiring compensatory hyperlordosis to shift the center of mass posteriorly back over the hip joints, often resulting in lower back pain (*34*). The last lumbar vertebra of *Au. sediba* has very high dorsal wedging, suggesting elevated lordosis (*6*), which may have adapted this species to the challenges of being a hyperpronating biped.

Although we find the evidence compelling that *Au. sediba*, or at least MH2, was a hyperpronating biped (Fig. 3 and Table 1), the selective advantage of this form of bipedality is unclear. There is little evidence that other known australopiths were hyperpronators, because the peculiar anatomies of the *Au. sediba* foot, knee, and hip are not found in earlier australopiths. Recent work on the Laetoli footprints (*47*, *48*) suggests that although the makers of the prints (presumably *Au. afarensis*) walked with a human-like gait, they had slightly less medial weight transfer. The hallux of *Au. afarensis* is domed and robust (*49*), indicating that weight transfer was more human-like than ape-like, but there probably were at least subtle differences in how *Au. afarensis* walked as compared to most modern humans. We hypothesize that terrestrial bipedalism in *Au. sediba* also differed subtly from that in most humans today, with *Au. sediba* engaging in more weight transfer on to the medial foot (hyperpronation) rather than less, as may have been the case with *Au. afarensis*.

Our interpretation of Malapa skeletal morphology extends the variation in *Australopithecus* locomotion. As suggested by others (*7*, *12*, *13*), there were different kinematic solutions for being a bipedal hominin in the Plio-Pleistocene. The MH2 skeleton provides insight into one of those potential solutions: hyperpronation. This mode of locomotion may be a compromise between an animal that is adapted for extended knee bipedalism and one that either still had an arboreal component or had re-evolved a more arboreal lifestyle from a more terrestrial ancestor. There is some postcranial evidence that the South African species *Au. africanus* may have been more arboreal than the east African *Au. afarensis* (*50*, *51*), and a hypothesized close relationship between *Au. africanus* and *Au. sediba* (*1*, *11*), along with features in the upper limbs of the latter thought to reflect adaptations to climbing and suspension (*3*, *4*), is consistent with a retained arboreal component in the locomotor repertoire of *Au. sediba*. Pronation is an important foot motion that shifts weight onto the medial side of the foot in climbing apes (*52*, *53*) and serves a role in weight transfer, shock absorption, and negotiation of uneven substrates during human bipedal gaits. An animal that was adapted to do both reasonably well may have had to support an increasingly mobile foot by evolving a large mobile medial column and important stabilizing anatomies at the knee and hip, in order to survive in these dual worlds.

References and Notes

1. L. R. Berger *et al.*, *Australopithecus sediba*: A new species of *Homo*-like australopith from South Africa. *Science* **328**, 195 (2010). doi: 10.1126/science.1184944; pmid: 20378811
2. R. Pickering *et al.*, *Australopithecus sediba* at 1.977 Ma and implications for the origins of the genus *Homo*. *Science* **333**, 1421 (2011). doi: 10.1126/science.1203697; pmid: 21903808
3. T. L. Kivell, J. M. Kibii, S. E. Churchill, P. Schmid, L. R. Berger, *Australopithecus sediba* hand demonstrates mosaic evolution of locomotor and manipulative abilities. *Science* **333**, 1411 (2011). doi: 10.1126/science.1202625; pmid: 21903806
4. S. E. Churchill *et al.*, The upper limb of *Australopithecus sediba*. *Science* **340**, 1233477 (2013). doi: 10.1126/science.1233477
5. P. Schmid *et al.*, Mosaic morphology in the thorax of *Australopithecus sediba*. *Science* **340**, 1234598 (2013). doi: 10.1126/science.1234598
6. S. Williams *et al.*, The vertebral column of *Australopithecus sediba*. *Science* **340**, 1232996 (2013). doi: 10.1126/science.1232996
7. B. Zipfel *et al.*, The foot and ankle of *Australopithecus sediba*. *Science* **333**, 1417 (2011). doi: 10.1126/science.1202703; pmid: 21903807
8. K. J. Carlson *et al.*, The endocast of MH1, *Australopithecus sediba*. *Science* **333**, 1402 (2011). doi: 10.1126/science.1203922; pmid: 21903804
9. J. M. Kibii *et al.*, A partial pelvis of *Australopithecus sediba*. *Science* **333**, 1407 (2011). doi: 10.1126/science.1202521; pmid: 21903805
10. D. J. de Ruiter *et al.*, Mandibular remains support taxonomic validity of *Australopithecus sediba*. *Science* **340**, 1232997 (2013). doi: 10.1126/science.1232997
11. J. D. Irish, D. Guatelli-Steinberg, S. S. Legge, L. R. Berger, D. J. de Ruiter, Dental morphology and the phylogenetic "place" of *Australopithecus sediba*. *Science* **340**, 1233062 (2013). doi: 10.1126/science.1233062
12. W. E. H. Harcourt-Smith, L. C. Aiello, Fossils, feet and the evolution of human bipedal locomotion. *J. Anat.* **204**, 403 (2004). doi: 10.1111/j.0021-8782.2004.00296.x; pmid: 15198703
13. Y. Haile-Selassie *et al.*, A new hominin foot from Ethiopia shows multiple Pliocene bipedal adaptations. *Nature* **483**, 565 (2012). doi: 10.1038/nature10922; pmid: 22460901
14. Methods and background are available as supplementary materials on *Science* Online.
15. C. O. Lovejoy, R. S. Meindl, J. C. Ohman, K. G. Heiple, T. D. White, The Maka femur and its bearing on the antiquity of human walking: Applying contemporary concepts of morphogenesis to the human fossil record. *Am. J. Phys. Anthropol.* **119**, 97 (2002). doi: 10.1002/ajpa.10111; pmid: 12237933
16. B. Asfaw, Proximal femur articulation in Pliocene hominids. *Am. J. Phys. Anthropol.* **68**, 535 (1985). doi: 10.1002/ajpa.1330680409; pmid: 3936365
17. C. Tardieu, Development of the human hind limb and its importance for the evolution of bipedalism. *Evol. Anthropol.* **19**, 174 (2010). doi: 10.1002/evan.20276
18. C. O. Lovejoy, The natural history of human gait and posture. Part 3. The knee. *Gait Posture* **25**, 325 (2007). doi: 10.1016/j.gaitpost.2006.05.001; pmid: 16766186
19. C. Tardieu *et al.*, Relationship between formation of the femoral bicondylar angle and trochlear shape: Independence of diaphyseal and epiphyseal growth. *Am. J. Phys. Anthropol.* **130**, 491 (2006). doi: 10.1002/ajpa.20373; pmid: 16425192
20. J. A. Wanner, Variations in the anterior patellar groove of the human femur. *Am. J. Phys. Anthropol.* **47**, 99 (1977). doi: 10.1002/ajpa.1330470117; pmid: 888940
21. W. E. Clark, Observations on the anatomy of the fossil Australopithecinae. *J. Anat.* **81**, 300 (1947). pmid: 17105037
22. K. G. Heiple, C. O. Lovejoy, The distal femoral anatomy of *Australopithecus*. *Am. J. Phys. Anthropol.* **35**, 75 (1971). doi: 10.1002/ajpa.1330350109; pmid: 5003051
23. C. Tardieu, Morpho-functional analysis of the articular surfaces of the knee-joint in primates, in *Primate Evolutionary Biology*, A. B. Chiarelli, R. S. Corruccini, Eds. (Springer-Verlag, New York, 1981), pp. 68–80.
24. L. C. Aiello, M. C. Dean, *An Introduction to Human Evolutionary Anatomy* (Academic Press, London, 1990).
25. J. M. Organ, C. V. Ward, Contours of the hominoid lateral tibial condyle with implications for *Australopithecus*. *J. Hum. Evol.* **51**, 113 (2006). doi: 10.1016/j.jhevol.2006.01.007; pmid: 16563467
26. B. Senut, C. Tardieu, Functional aspects of Plio-Pleistocene hominid limb bones: Implications for taxonomy and phylogeny, in *Ancestors: The Hard Evidence*, E. Delson, Ed. (Alan R. Liss, New York, 1985), pp. 193–201.

27. J. Dugan, T. W. Holliday, Utility of the lateral meniscal notch in distinguishing hominin taxa. *J. Hum. Evol.* **57**, 773 (2009). doi: 10.1016/j.jhevol.2009.07.006; pmid: 19878967
28. Pronation of the foot is a triplanar motion (eversion, abduction, and dorsiflexion occurring simultaneously) and is a normal function of bipedal foot mechanics in order to absorb ground reaction forces and accommodate uneven substrates. It converts the foot from a rigid structure at heel strike to a more mobile one at midstance. Hyperpronation is poorly defined in a clinical sense, because there is no distinct cutoff between those that excessively pronate and those that do not. However, here we define it as continued pronation into the part of stance phase when the foot should be resupinating (usually at the later part of midstance and during the entire propulsive phase). Extended (timing-wise) pronation is caused both by the magnitude of pronation (in degrees) that occurs as a result of the large pronatory torque generated by contacting the ground on a varus heel and forefoot, and the timing of foot motion. Because of the excessive motion occurring at the subtalar, midtarsal, and tarsometatarsal joints, the foot fails to resupinate at late stance and pushoff.
29. D. L. Gebo, Plantigrady and foot adaptation in African apes: Implications for hominid origins. *Am. J. Phys. Anthropol.* **89**, 29 (1992). doi: 10.1002/ajpa.1330890105; pmid: 1530061
30. H. Elftman, J. Manter, Chimpanzee and human feet in bipedal walking. *Am. J. Phys. Anthropol.* **20**, 69 (1935). doi: 10.1002/ajpa.1330200109
31. E. Vereecke, K. D'Août, D. De Clercq, L. Van Elsacker, P. Aerts, Dynamic plantar pressure distribution during terrestrial locomotion of bonobos (*Pan paniscus*). *Am. J. Phys. Anthropol.* **120**, 373 (2003). doi: 10.1002/ajpa.10163; pmid: 12627532
32. C. O. Lovejoy, B. Latimer, G. Suwa, B. Asfaw, T. D. White, Combining prehension and propulsion: The foot of *Ardipithecus ramidus*. *Science* **326**, 72e1-e8 (2009).
33. K. D. Gross *et al*., Varus foot alignment and hip conditions in older adults. *Arthritis Rheum.* **56**, 2993 (2007). doi: 10.1002/art.22850; pmid: 17763430
34. K. G. Holt, J. Hamill, Running injuries and treatment: A dynamic approach, in *Rehabilitation of the Foot and Ankle*, G. J. Sammarco, Ed. (Mosby, St. Louis, MO, 1995), pp. 241–258.
35. L. Wong, A. Hunt, J. Burns, J. Crosbie, Effect of foot morphology on center-of-pressure excursion during barefoot walking. *J. Am. Podiatr. Med. Assoc.* **98**, 112 (2008). pmid: 18347119
36. T. C. Michaud, The foot: Hyperpronation and hypopronation, in *Functional Soft-Tissue Examination and Treatment by Manual Methods*, W. I. Hammer, Ed. (Jones and Bartlett, Sudbury, MA, 2005), pp. 399–426.
37. K. A. Kirby, Subtalar joint axis location and rotational equilibrium theory of foot function. *J. Am. Podiatr. Med. Assoc.* **91**, 465 (2001). pmid: 11679628
38. M. B. Bennett, R. F. Ker, The mechanical properties of the human subcalcaneal fat pad in compression. *J. Anat.* **171**, 131 (1990). pmid: 2081699
39. T. J. Ouzounian, M. J. Shereff, In vitro determination of midfoot motion. *Foot Ankle* **10**, 140 (1989). doi: 10.1177/107110078901000305; pmid: 2613125
40. J. M. DeSilva, Revisiting the "midtarsal break." *Am. J. Phys. Anthropol.* **141**, 245 (2010). pmid: 19672845
41. C. V. Ward, W. H. Kimbel, D. C. Johanson, Complete fourth metatarsal and arches in the foot of *Australopithecus afarensis*. *Science* **331**, 750 (2011). doi: 10.1126/science.1201463; pmid: 21311018
42. D. Tiberio, The effect of excessive subtalar joint pronation on patellofemoral mechanics: A theoretical model. *J. Orthop. Sports Phys. Ther.* **9**, 160 (1987). pmid: 18797010
43. S. Khamis, Z. Yizhar, Effect of feet hyperpronation on pelvic alignment in a standing position. *Gait Posture* **25**, 127 (2007). doi: 10.1016/j.gaitpost.2006.02.005; pmid: 16621569
44. C. M. Powers, R. Maffucci, S. Hampton, Rearfoot posture in subjects with patellofemoral pain. *J. Orthop. Sports Phys. Ther.* **22**, 155 (1995). pmid: 8535473
45. B. A. Rothbart, L. Estabrook, Excessive pronation: A major biomechanical determinant in the development of chondromalacia and pelvic lists. *J. Manipulative Physiol. Ther.* **11**, 373 (1988). pmid: 2976805
46. J. J. Eng, M. R. Pierrynowski, Evaluation of soft foot orthotics in the treatment of patellofemoral pain syndrome. *Phys. Ther.* **73**, 62, discussion 68 (1993). pmid: 8421719
47. M. R. Bennett *et al*., Early hominin foot morphology based on 1.5-million-year-old footprints from Ileret, Kenya. *Science* **323**, 1197 (2009). doi: 10.1126/science.1168132; pmid: 19251625
48. R. H. Crompton *et al*., Human-like external function of the foot, and fully upright gait, confirmed in the 3.66 million year old Laetoli hominin footprints by topographic statistics, experimental footprint-formation and computer simulation. *J. R. Soc. Interface* **9**, 707 (2012). doi: 10.1098/rsif.2011.0258; pmid: 21775326
49. B. Latimer, C. O. Lovejoy, Hallucal tarsometatarsal joint in *Australopithecus afarensis*. *Am. J. Phys. Anthropol.* **82**, 125 (1990). doi: 10.1002/ajpa.1330820202; pmid: 2360609
50. H. M. McHenry, L. R. Berger, Body proportions of *Australopithecus afarensis* and *A. africanus* and the origin of the genus *Homo*. *J. Hum. Evol.* **35**, 1 (1998). doi: 10.1006/jhev.1997.0197; pmid: 9680464
51. D. J. Green, A. D. Gordon, B. G. Richmond, Limb-size proportions in *Australopithecus afarensis* and *Australopithecus africanus*. *J. Hum. Evol.* **52**, 187 (2007). doi: 10.1016/j.jhevol.2006.09.001; pmid: 17049965
52. J. T. Stern Jr., R. L. Susman, The locomotor anatomy of *Australopithecus afarensis*. *Am. J. Phys. Anthropol.* **60**, 279 (1983). doi: 10.1002/ajpa.1330600302; pmid: 6405621
53. R. Wunderlich, thesis, State University of New York at Stony Brook, Stony Brook, NY (1999).

Acknowledgments: We thank the South African Heritage Resource agency for the permits to work at the Malapa site; the Nash family for granting access to the Malapa site and continued support of research on their reserve; the South African Department of Science and Technology and the African Origins Platform (AOP), the South African National Research Foundation, the Evolutionary Studies Institute, the University of the Witwatersrand, the University of the Witwatersrand's Vice Chancellor's Discretionary Fund, the National Geographic Society, the Leakey Foundation, the Palaeontological Scientific Trust, the Andrew W. Mellon Foundation, the Ford Foundation, the U.S. Diplomatic Mission to South Africa, the French Embassy of South Africa, the A.H. Schultz Foundation, Boston University, Duke University, a Ray A. Rothrock '77 Fellowship and International Research Travel Assistance Grant of Texas A&M University, and the Oppenheimer and Ackerman families and Sir Richard Branson for funding; the University of the Witwatersrand's Schools of Geosciences and Anatomical Sciences and the Bernard Price Institute for Palaeontology for support and facilities; the Gauteng Government, Gauteng Department of Agriculture, Conservation and Environment and the Cradle of Humankind Management Authority; and our respective universities for ongoing support. We thank the VIP lab of the Palaeosciences Centre and the Microfocus X-ray CT facility of the Palaeosciences Centre at Wits; and for funding these facilities, we thank the University of the Witwatersrand Office of Research and the National Research Foundation Strategic Research Infrastructure Grant and AOP funding programs. For access to comparative specimens, we thank E. Mbua, P. Kiura, V. Iminjili, and the National Museums of Kenya; A. Kwekason, P. Msemwa, and the Tanzania Commission for Science and Technology; B. Billings, Fossil Primate Access Advisory and the School of Anatomical Sciences at the University of the Witwatersrand; S. Potze, L. C. Kgasi, and the Ditsong Museum; Y. Haile-Selassie, L. Jellema, and the Cleveland Museum of Natural History; J. Chupasko and the Harvard Museum of Comparative Zoology; D. Pilbeam, M. Morgan, O. Herschensohn, J. Rousseau, and the Harvard Museum of Archeology and Ethnology; E. Westwig and the American Museum of Natural History; M. Wolpoff and the Department of Anthropology at the University of Michigan; and O. Lovejoy (Kent State University). For technical and material support, we thank Duke University and the University of Zurich 2009 and 2010 Field Schools. Numerous individuals have been involved in the ongoing preparation and excavation of these fossils, including C. Dube, C. Kemp, M. Kgasi, M. Languza, J. Malaza, G. Mokoma, P. Mukanela, T. Nemvhundi, M. Ngcamphalala, S. Jirah, S. Tshabalala, and C. Yates. Other individuals who have given significant support to this project include B. de Klerk, W. Lawrence, C. Steininger, B. Kuhn, L. Pollarolo, J. Kretzen, D. Conforti, J. McCaffery, C. Dlamini, H. Visser, R. McCrae-Samuel, B. Nkosi, B. Louw, L. Backwell, F. Thackeray, and M. Peltier. J. Smilg facilitated medical CT scanning of the specimens. The *Au. sediba* specimens are archived at the Evolutionary Studies Institute at the University of the Witwatersrand. All data used in this study are available upon request, including access to the original specimens, by bona fide scientists.

Supplementary Materials

www.sciencemag.org/content/340/6129/1232999/suppl/DC1
Materials and Methods
Supplementary Text
Figs. S1 to S15
Tables S1 to S3
References (*54*–*78*)

20 November 2012; accepted 13 March 2013
10.1126/science.1232999

Supplementary Materials for

The Lower Limb and Mechanics of Walking in *Australopithecus sediba*

Jeremy M. DeSilva,* Kenneth G. Holt, Steven E. Churchill, Kristian J. Carlson, Christopher S. Walker, Bernhard Zipfel, Lee R. Berger

*Corresponding author. E-mail: jdesilva@bu.edu

Published 12 April 2013, *Science* **340**, 1232999 (2013)
DOI: 10.1126/science.1232999

This PDF file includes:

Metric analysis of lower limb elements.

Materials and methods: The lateral trochlear groove angle (Fig. 1) was measured following a published protocol (*19*, *20*). Fossils were photographed in inferior view, the photographs were imported into Image J (NIH) (*54*) and an angle was taken between a line connecting the most anterior point of the lateral patellar lip and the most posterior point of the patellar groove and a horizontal. The lateral trochlear angle obtained from fossil hominin femora was compared to data reported elsewhere (*20*). To test the validity of the measurement, twenty human distal femora from the 15th and 16th century Mistihalj collection of Montenegro (Harvard Museum of Archaeology and Ethnology) were measured and compared to the results in *20*. The angle in *20* is 17.33° ± 4.6° (n=32). The angle of the distal femora from Mistihalj was 15.89° ± 3.8° (n=20). The difference is statistically non-significant (p=0.25) and therefore the results reported in Fig. 1 reflect the larger sample from *20*.

The anterior expansion of the patellar surface (fig. S8) was measured on the same photographs of these 20 Mistihalj femora in inferior view. Using the line tool in Image J, horizontal lines were drawn through the most anterior point of the intercondylar groove and the most posterior aspect of the femoral condyles. The projected distance from the deepest point of the patellar groove to the most anterior point of the intercondylar groove was divided by the total distance from the most posterior aspect of the patellar groove and the most posterior aspect of the femoral condyles (as illustrated in fig. S8).

Measurements taken on the proximal femur (table S2) followed those reported elsewhere (*15*, *55*, *56*). Human measurements were obtained from several collections: Libben (Kent State University), Mistihalj (Harvard Museum of Archaeology and Ethnology), and an unprovenienced collection in the Department of Anthropology at the University of Michigan. Chimpanzee and gorilla femora were measured at the Harvard Museum of Comparative Zoology, American Museum of Natural History, and Cleveland Museum of Natural History. All of the ape measurements were done on adult, wild-shot specimens. Fibulae of humans (n=30), chimpanzees (n=10), and gorillas (n=10) were measured at the Cleveland Museum of Natural History, American Museum of Natural History, and Harvard Museum of Archaeology and Ethnology. Patellae of humans (n=46), chimpanzees (n=10), and gorillas (n=10) were measured at the Cleveland Museum of Natural History, American Museum of Natural History, Harvard Museum of Archaeology and Ethnology, Boston University Biological Anthropology Laboratory, and Dart Collection at the University of the Witwatersrand. The convexity of the fourth metatarsal (Fig. 4) was measured as described in *40*.

Observations reported in this paper were made on original fossils at the Kenya National Museum, Tanzania National Museum and House of Culture, Ditsong Museum of Natural History (Pretoria), and the University of the Witwatersrand. Fossil casts of material from Ethiopia were studied at the Cleveland Museum of Natural History and Harvard Museum of Archaeology and Ethnology, and checked against published descriptions in *57* and *58*. Data on material from *Orrorin*, Dmanisi, Bouri, and *H. floresiensis* were obtained from published reports.

Table S1: Lower limb remains attributed to *Australopithecus sediba*

Catalogue number	Individual	Element	Notes
U.W. 88-4	MH1	Right proximal femur	Conjoins with *U.W. 88-5, 39*
U.W. 88-5	MH1	Right femoral shaft fragment	Conjoins with *U.W. 88-4*
U.W. 88-16	MH1?	Right 5th MT	
U.W. 88-18	MH1	Left fibular shaft fragment	
U.W. 88-21	MH4	Right distal tibia with shaft	Conjoins with *U.W. 88-40*
U.W. 88-22	MH1?	Right 4th MT	
U.W. 88-23	MH2	Left proximal fibula	Conjoins with *U.W. 88-84*
U.W. 88-24	MH2	Left proximal tibial fragment	
U.W. 88-33	MH2?	Right 5th MT	
U.W. 88-39	MH1	Right femoral head epiphysis	Conjoins with *U.W. 88-4*
U.W. 88-40	MH4	Right tibial shaft fragment	Conjoins with *U.W. 88-21*
U.W. 88-51	MH2	Right proximal femur	
U.W. 88-53	MH2	Right femoral shaft fragment	
U.W. 88-63	MH2	Right distal femur	
U.W. 88-64	MH2	Right proximal tibia	Conjoins with *U.W. 88-78*
U.W. 88-78	MH2	Right proximal tibia	Conjoins with *U.W. 88-64*
U.W. 88-79	MH2	Right patella	Conjoins with *U.W. 88-100*
U.W. 88-84	MH2	Left fibular shaft fragment	Conjoins with *U.W. 88-23, 146*
U.W. 88-89	MH1	Right tibial shaft fragment	
U.W. 88-97	MH2	Right distal tibia	Fused with *U.W. 88-98,99*
U.W. 88-98	MH2	Right talus	Fused with *U.W. 88-97,99*
U.W. 88-99	MH2	Right calcaneus	Fused with *U.W. 88-97,98*
U.W. 88-100	MH2	Right patellar fragment	Conjoins with *U.W. 88-79*
U.W. 88-113	MH1	Calcaneal apophysis	
U.W. 88-139	MH2?	Left lateral cuneiform	
U.W. 88-146	MH2	Left fibular fragment	Conjoins with *U.W. 88-84, 202*
U.W. 88-202	MH2	Left fibular fragment	Conjoins with *U.W. 88-146*

Table S2: Comparative femur dimensions. Measurements taken on original specimens unless noted otherwise.

Specimen	Species	Head diameter (mm)	Neck shape (SI/ML)*100	Neck-shaft angle (°)	Biomechanical neck length (mm)	BNL/HD	Platymeric index
	Homo sapiens	44.7 ± 4.0 (n=183)	82.4 ± 5.8 (n=183)	124.4 ± 3.8 (n=100)	68.6 ± 5.2 (n=68)	1.55 ± 0.08 (n=68)	74.6 ± 5.6 (*15*)
	Pan troglodytes	33.4 ± 2.3 (n=101)	85.4 ± 4.9 (n=101)	124.1 ± 4.6 (n=20)	51.1 ± 3.7 (n=42)	1.56 ± 0.07 (n=42)	83.6 ± 5.9 (*15*)
	Gorilla gorilla	43.9 ± 5.4 (n=95)	79.7 ± 5.3 (n=95)	119.0 ± 4.3 (n=20)	68.8 ± 9.6 (n=47)	1.58 ± 0.08 (n=47)	86.3 ± 3.2 (*15*)
U.W. 88-4,5,39 (MH1)	*Australopithecus sediba*	33.0 (est)	73.4	110-115	60.3	1.83	77.0
U.W. 88-51 (MH2)	*Australopithecus sediba*	32.7	74.0 (min)	-	-	-	-
BAR 1002'00 (*59*)	*Orrorin tugenensis*	32.1	69.3	125	54*	1.70	82.4
BAR 1003'00 (*59*)	*O. tugenensis*	-	60.6	-	-	-	-
BAR 1215'00 (*59*)	*O. tugenensis*	-	61.8	-	-	-	-
A.L. 152-2 (*60*)	*Au. afarensis*	33.1	-	125	-	-	-
A.L. 211-1 (*57*)	*Au. afarensis*	-	-	-	-	-	77.3
A.L. 288-1 (*58*)	*Au. afarensis*	28.6	69.6	123	47.3	1.65	67.8
A.L. 333-3 (*57*)	*Au. afarensis*	39.4	79.6	125	63.0	1.54	75.5
A.L. 333-95 (*57*)	*Au. afarensis*	-	68.7	-	-	-	-
A.L. 333-142 (*60*)	*Au. afarensis*		78.7				
A.L. 827-1 (*60*)	*Au. afarensis*	38.2	87.9	119	-	-	-
MAK-VP 1/1 (*15*)	*Au. afarensis*	-	-	117	-	-	71.6
BOU-VP-12/1 (*61*)	*Au. garhi?*	-	-	134 (est)	-	-	75.0
KNM-WT 16002	*Australopithecus*?	-	64.4	-	-	-	70.9
MLD 46 (*55*)	*Au. africanus*	36.0	73.4	120	63.5	1.76	-
Sts 14 (*56*)	*Au. africanus*	-	-	118	53.0	-	-
StW 25	*Au. africanus*	30.4	-	-	-	-	-
StW 99	*Au. africanus*	39.7 (est) 35.5 (min)	69.1	113	72.6	1.83	74.9
StW 361	*Au. africanus*	29.1 (est)	-	-	-	-	-
StW 392	*Au. africanus*	31.5	-	-	-	-	-
StW 403	*Au. africanus*	31.1	63.1	-	-	-	-
StW 479	*Au. africanus*	31.0 (est)	76.7 (max)	-	-	-	-
StW 501	*Au. africanus*	31.7	73.9 (est)	-	-	-	-
StW 522	*Au. africanus*	30.9	70.2	124	43.4 (est)	1.41 (est)	79.3 (est)
StW 527	*Au. africanus*	32.2	-	-	-	-	-
StW 598 (*62*)	*Au. africanus*	32.2	61.5	116	63.0*	1.96	-
StW 311	*Homo?*	35.7	71.8 (min)	-	-	-	-

SK 97	*Paranthropus robustus*	37.3	72.1	118 (*63*)	67.0	1.80	73.8
SK 82	*P. robustus*	34.2	71.3	120 (*63*)	64.0	1.87	81.7
SK 14024	*P. robustus*	31.3	71.4	-	-	-	-
SK 3121	*P. robustus*	28.6	72.0	-	-	-	-
SKW 19	*P. robustus*	30.4	-	-	-	-	-
SWT1/LB-2 (*64*)	*P. robustus*	34.4	68.3	-	-	-	-
OH 20	*P. boisei*		67.1	~115 (*63*)	78.0 (*56*)	-	76.1
KNM-ER 738	*P. boisei?*	33.2	75.6	115 (*63*)	54.0 (*56*)	1.63	81.6
KNM-ER 815	*P. boisei?*	-	54.0	~115 (*63*)	-	-	74.3
KNM-ER 1465	*P. boisei?*	-	-	-	-	-	86.6
KNM-ER 1500	*P. boisei?*	-	-	-	-	-	80.0
KNM-ER 1503	*P. boisei?*	35.4	59.5	114 (*65*)	70.6	1.99	73.5
KNM-ER 1505	*P. boisei?*	35.4	67.8	-	-	-	-
KNM-ER 1463	Hominin	-	68.5	-	-	-	80.1
KNM-ER 1475	Hominin	-	87.1	125 (*66*)	-	-	89.7
KNM-ER 1809	Hominin		-	-	-	-	79.4
KNM-ER 5880	Hominin	-	68.3		-	-	76.2
KNM-ER 3728	*Homo?*	-	56.9		~68	-	61.4
KNM-ER 1481	*Homo?*	42.1	79.9	123 (*66*)	68.8	1.63	74.7
KNM-ER 1472	*Homo?*	38.6	81.6	125 (*66*)	60.2	1.56 (max)	69.6
OH 62	*Homo habilis?*	-	-	123 (*67*)	-	-	97.6
D4167 (*68*)	*H. erectus*	40.0	66.2	-	67.7*	1.69	-
KNM-ER 736	*H. erectus?*	-	-	-	-	-	79.0
KNM-ER 737	*H. erectus?*	-	-	-	-	-	71.2
KNM-ER 803	*H. erectus*	-	-	-	-	-	82.1
KNM-WT 15000 (*69*)	*H. erectus*	46.0	70.6	110	84.0	1.83	73.2
OH 34	*H. erectus?*	-	65.0		-	-	81.9
OH 28	*H. erectus*	-	-	-	-	-	66.1
BOU-VP-1/75 (*70*)	*H. erectus*	-	-	-	-	-	66.2
BOU-VP-19/63 (*70*)	*H. erectus*	-	-	-	-	-	75.1
KNM-ER 999	*Homo*	44.8 (est)	-	135 (*71*)	77.5	1.73 (max)	89.1
Berg Aukas	*Homo*	58.0	94.9	106 (*72*)	80.9	1.39	73.5
LB 1 (*73*)	*H. floresiensis*	31.0	65.0	128	55.5*	1.79	81.3

*Estimated from published photographs

Table S3: Bicondylar angle in extant apes and fossil hominins

Specimen	Species	Geological age (Ma)	Bicondylar angle (°)	Source
	Pan troglodytes	Present	0.97 (1.93)	*24*
	Gorilla gorilla	Present	1.72 (3.80)	*24*
	Homo sapiens (male)	Present	9.43 (1.93)	*24*
	Homo sapiens (female)	Present	10.5 (2.4)	*24*
U.W. 88-63	*Australopithecus sediba*	1.977	~9	This study
A.L. 129-1	*Au. afarensis*	3.4	15	*24*
A.L. 333-4	*Au. afarensis*	3.2	9	*24*
Sts 34	*Au. africanus*	2.0-2.6	15	*24*
TM 1513	*Au. africanus*	2.0-2.6	14	*24*
KNM-ER 1472	*Homo* sp.	1.89	13	*66*
KNM-ER 1481	*Homo* sp.	1.89	10	*66*
KNM-ER 3951	*Homo* sp.?	1.89	15	*74*
KNM-ER 1592	*Homo* sp.?	1.85	~10	*74*
D4167	*Homo erectus*	1.77	8.5	*68*
KNM-ER 993	*Paranthropus*?	1.53	14.5	*24*
KNM-WT 15000	*Homo erectus*	1.53	10	*68*
LB 1	*Homo floresiensis*	0.017	14	*73*

Fig. S1. Proximal femur of (left) MH1 (*U.W. 88-4, 5, 39*) and (right) MH2 (*U.W. 88-51*). MH1 femoral head epiphyseal surface is shown at the top left, followed by medial and anterior views (top). Below are lateral and posterior views of the conjoined *U.W. 88-4, 5, 39* femur. On the right hand side, MH2 is shown (top, left to right) in lateral, posterior, and medial views. Below (from top to bottom) are inferior, anterior, and superior views.

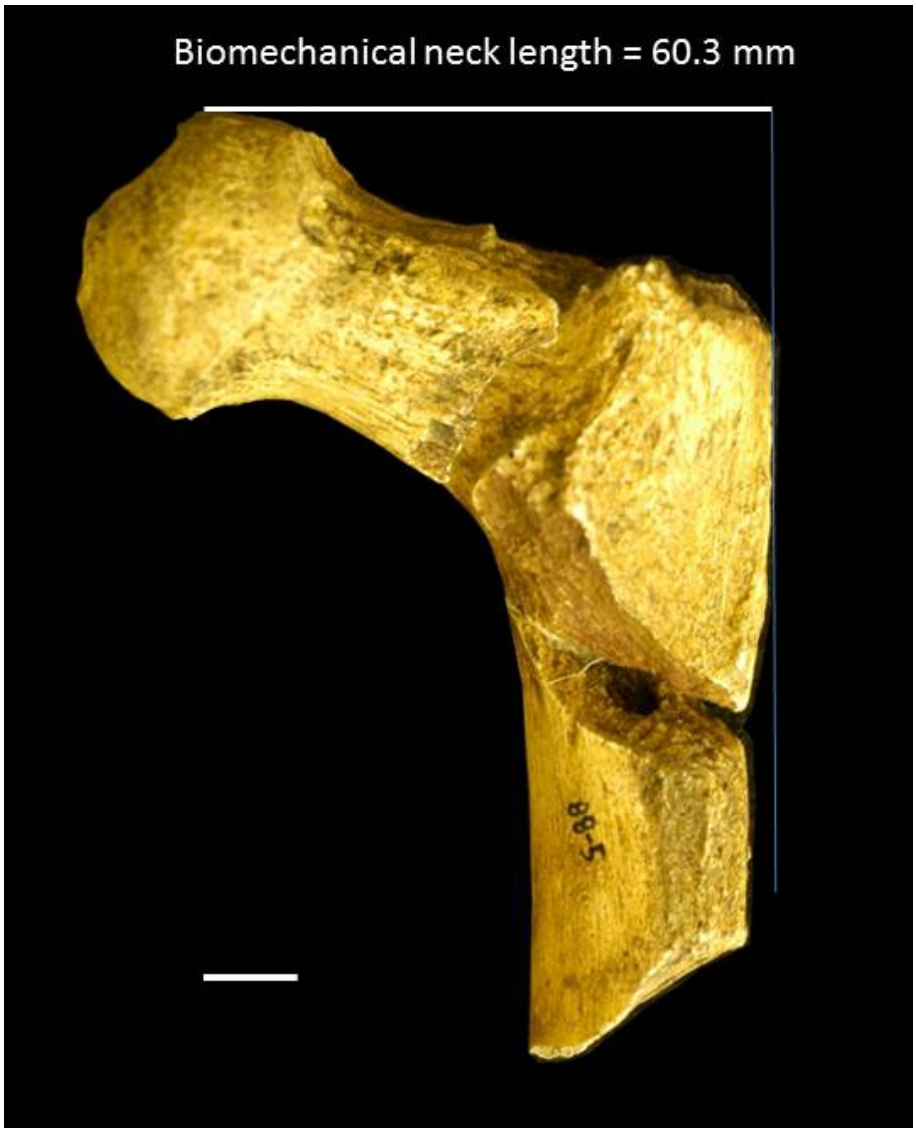

Fig. S2. The biomechanical neck length was calculated for MH1 by superimposing the MH2 head and neck onto the preserved femur of MH1 (see fig. S1 for the relative contributions of the MH1 and MH2 femora to this composite). The resulting composite right femur is illustrated above in posterior view. The superimposition was achieved by aligning the head-epiphysis junction on the MH2 adult with the preserved epiphyseal surface of the MH1 femur (*U.W. 88-4*). No scaling was necessary since the dimensions of the two femora are quite similar (table S2). Scale bar is 1 cm.

Fig. S3. The distal femur of MH2 (*U.W. 88-63*) shown in (from left to right) lateral, anterior, medial, and posterior views. Below is the femur shown inferiorly. Notice the exceptionally high lateral patellar lip and deep popliteal groove.

Fig. S4. Proximal tibia and patella of *Au. sediba*. Top image is *U.W. 88-64*, the lateral most portion of the tibial plateau of MH2 in (from left to right) lateral, medial, and posterior views. At bottom is an image of the proximal tibial plateau in superior view with *U.W. 88-64* (fragment to right) attached to *U.W. 88-78*. Cemented to *U.W. 88-78* is a part of the patella (*U.W. 88-79*), coming out of the image towards the camera. *U.W. 88-100* (not shown here) is a patellar fragment that conjoins with *U.W. 88-79* to form a nearly complete patella (see fig. S5).

Fig. S5. Reconstructed patella from MH2 shown in (top left to right) distal and proximal views, and (bottom left to right): medial, anterior, posterior, and lateral views. The fossil is in two pieces- the most medial and distal portion (seen best in the anterior and posterior views) is *U.W.88-100*. *U.W. 88-79* (the lateral and proximal portion of the patella) remains embedded in calcified matrix adhering to the proximal tibia of MH2 (*U.W. 88-78*). *U.W. 88-79* has been digitally segmented from µCT scans, and was rejoined to *U.W. 88-100* by aligning not only the clean articulations along the broken surface, but by also aligning the individual exposed trabeculae at the point of the break. The scale bar at the bottom of the image is 1 cm.

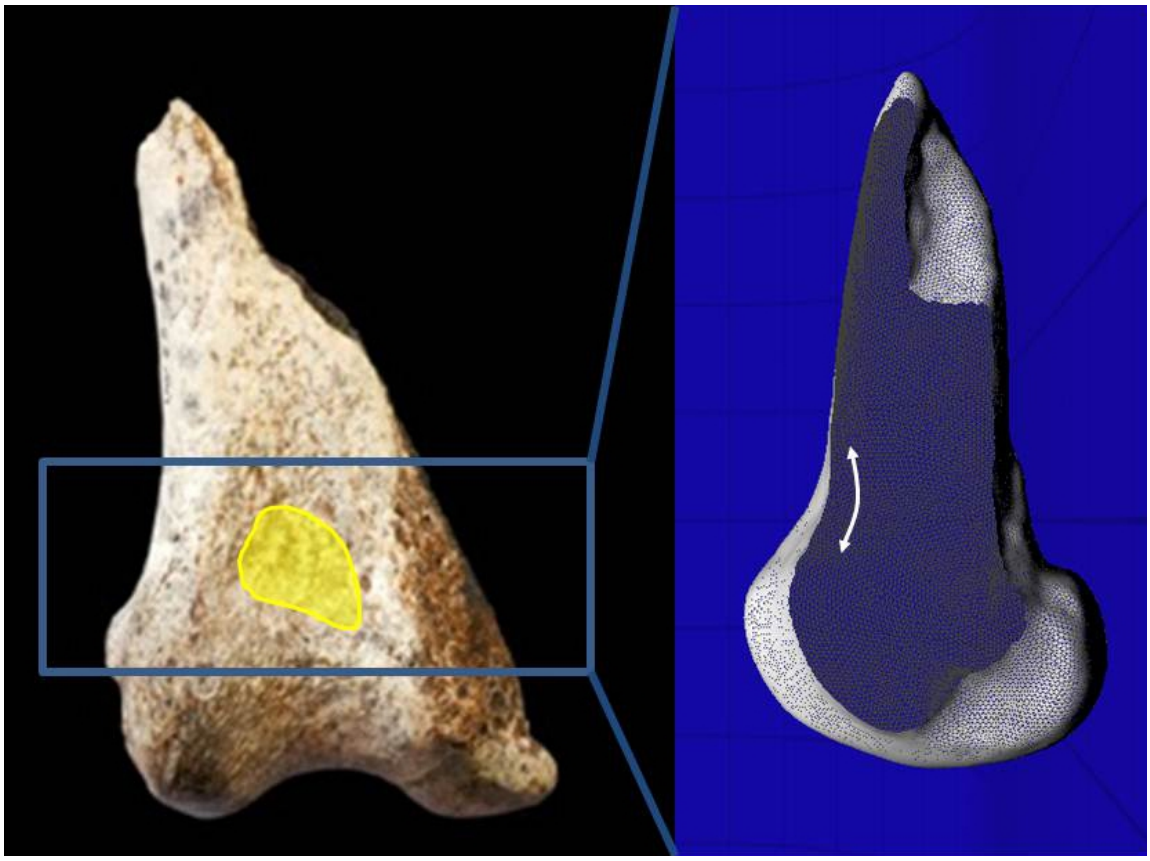

Fig. S6. The sustrochlear hollow (from *17*) is a palpable indentation just superior to the patellar articular surface. It receives the patella during full leg extension and is evidence for an extended leg during bipedal gait. The sustrochlear hollow in *Australopithecus sediba* is illustrated here in yellow. To the right is a digitally sectioned 3D surface scan of the *U.W. 88-63* femur sagitally-sectioned to show (with arrows) the sustrochlear hollow depression. This impression was also palpated and observed using sectioned 3D scans in all *Au. afarensis* femora (A.L. 129-1, A.L. 333w-56, A.L. 333-61) for which this region is preserved suggesting an extended leg during gait in this hominin. Other fossils (KNM-ER 993, KNM-ER 1472, KNM-ER 1481, KNM-ER 3951, KNM-WT 15000) also have a palpable sustrochlear hollow.

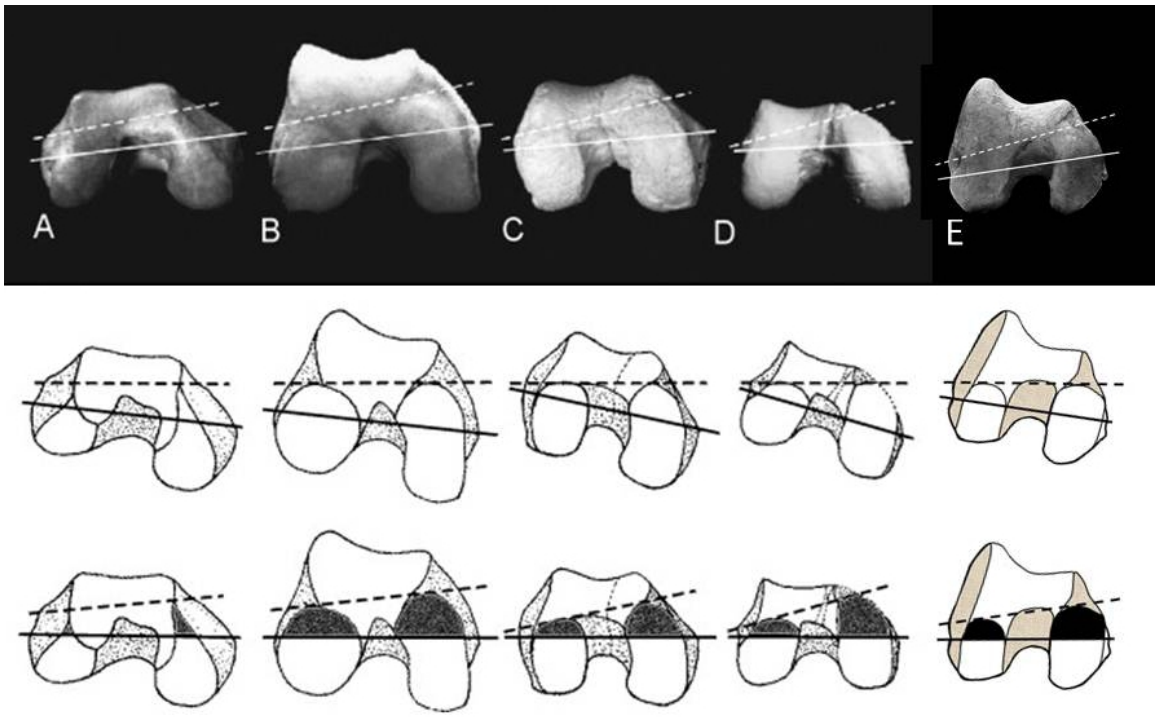

Fig. S7. The comparative anatomy of the ape, human, and fossil hominin distal femur as illustrated in (*18*). Distal femora are shown in inferior view above: A. Chimpanzee; B. Human; C: A.L. 333-4 (*Au. afarensis*); D: A.L. 129-1 (*Au. afarensis*); E. *U.W. 88-63* (*Au. sediba*). A dotted line connects the meniscal grooves and a solid line runs through the epicondyles. In the second row, the meniscal groove dotted line is horizontal, showing the high lateral lipping (for patellar retention) in humans and fossil hominins. In this view, notice the exceptionally high lateral lip in *Au. sediba*. In the bottom row specimens are aligned by the epicondylar axis, and the articular surface of the femur anterior to the epicondylar line is shaded, indicating the "tibial dominant" nature of the hominin knee (*18*), evidence for full extension during gait. Reproduced with permission from Lovejoy 2005.

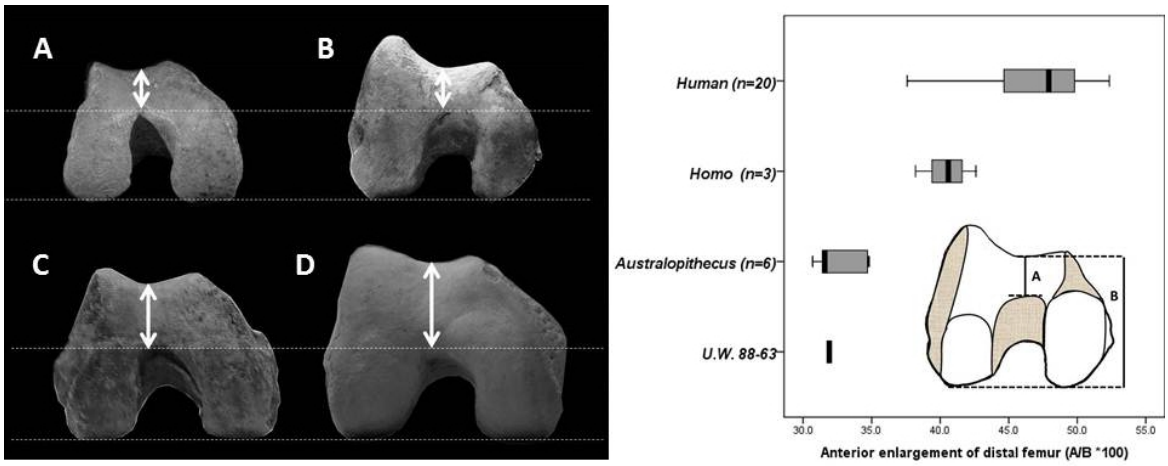

Fig. S8. The exceptionally high lateral lip in the *Au. sediba* femur is not a result of general anterior enlargement of the patellar surface. On the left are four femora: A. TM 1513 (*Au. africanus*); B. *U.W. 88-63* (*Au. sediba*); C. KNM-ER 1472 (*Homo* sp.); D. Modern human. Horizontal lines have been drawn through the most anterior point of the intercondylar groove and the most posterior aspect of the femoral condyles. The femora have been proportionately scaled so that the distance between these lines is the same in all four femora. Notice that anterior elongation of the patellar surface (indicated by white lines with arrowheads; A on the right) is quite reduced in australopiths (TM 1513 and *U.W. 88-63*) compared to fossil *Homo* and modern humans. To the right is a quantification of this anatomy showing (as suggested in *18*) that the anterior enlargement of the patellar surface is a *Homo*-feature. This anatomy increases the moment arm for the quadriceps, improving the mechanical advantage of this muscle.

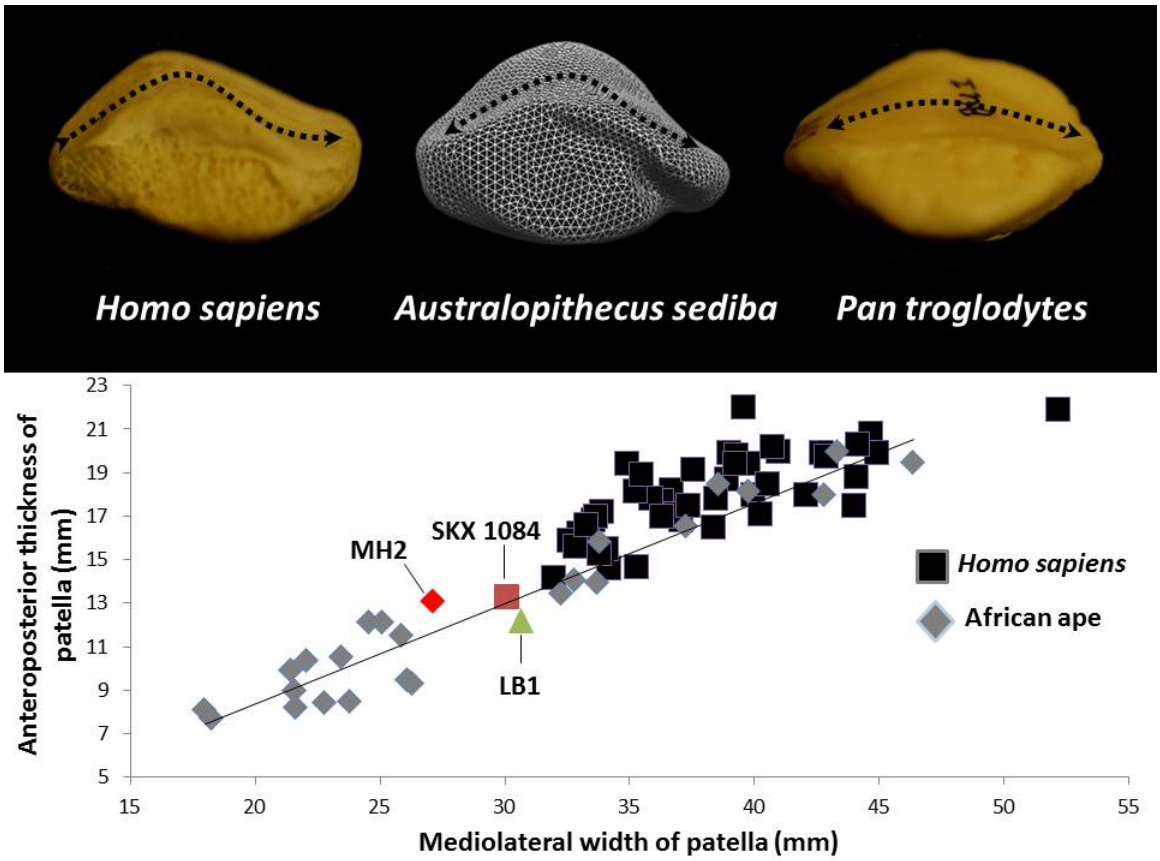

Fig. S9. Top images are scaled to the same mediolateral width. Human patellae and the patella from *Australopithecus sediba* are strongly convex posteriorly, whereas ape patellae tend to be flatter. This topography is related to the high lateral lip found in human distal femora. The bottom graph plots the maximum mediolateral width of the patella against the anteroposterior thickness. Relative to the width, humans tend to have slightly thicker patellae. Humans in this graph include small-bodied individuals from Merida, Mexico (Harvard Museum of Archaeology and Ethnology) and the San and Khoi-Khoi populations (Dart Collection, University of the Witwatersrand). The *Au. sediba* patella falls above the ape regression line. The patella from Swartkrans (SKX 1084) falls directly on the ape regression, whereas the patella of *Homo floresiensis* (data from *73*) falls below. Note, however, that the MH2 patella is strikingly narrow mediolaterally, narrower than LB1 even though MH2 is larger than LB1 in other skeletal dimensions (femoral head diameter, for example).

Fig. S10. MH2 fibula (*U.W. 88-23*, *-84*) in (from left to right) lateral, anterior, medial, and posterior views. *U.W. 88-146* and *U.W. 88-202* conjoin distally with *U.W. 88-84*, and the four pieces are shown in lateral view on the far right. The arrow points to an osteophytic outgrowth at the biceps femoris insertion. We hypothesize that this bony growth indicates that this muscle was overstrained during the hyperpronating gait of *Au. sediba*.

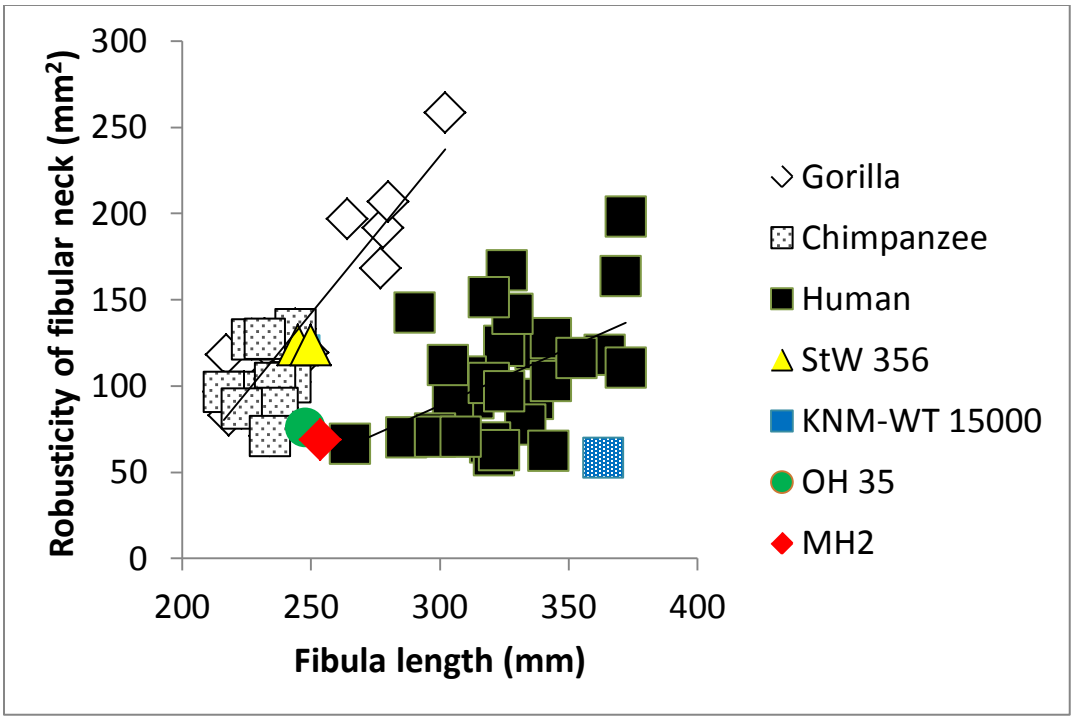

Fig. S11. Relative to the robusticity of the fibular neck (y-axis), humans have significantly longer fibulae than do African apes. Fibular robusticity is assessed here as the product of the anteroposterior and mediolateral minimum diameters of the neck. No fossil fibula from the Plio-Pleistocene is complete enough to get a definitive length. However, stature equations in (*75*) can be used to show that the fibula is approximately 4% shorter than the tibia in modern humans. The length of the tibia is known in KNM-WT 15000 (*69*), and estimated in OH 35 (*76*). We estimated the length of the MH2 tibia by comparing linear articular dimensions of the MH2 distal tibia to the MH4 distal tibia. The MH2 distal tibia is approximately 98% the size of MH4, suggesting a total length of approximately 264 mm and a fibula length of approximately 254 mm. The most complete fossil fibula from *Australopithecus* is StW 356, from Member 4, Sterkfontein. Both ends are missing; however, the proximal break occurs at the fibula neck, and the distal end is broken just superior to the talar facet. Using MH2 proximally and Lucy (A.L. 288-1) distally to derive separate estimates, the length of the fibula can be approximated to 245-250 mm (it is thus represented twice on the plot). StW 356 is quite robust, in the modern ape range. KNM-WT 15000 is human-like in its length and gracility. OH 35 and MH2 are slightly more gracile for their length than what is typically found in apes, and are closer to the human regression line. Humans in this graph include small-bodied individuals from Merida, Mexico (Harvard Museum of Archaeology and Ethnology).

Fig. S12. The total length of the MH4 tibia (*U.W. 88-21* and *U.W. 88-40*) was estimated as is shown in this image. The sediment block from which the *U.W. 88-40* proximal tibial shaft was recovered is shown here both with (middle) and without (left) the fossil in position. The block preserves an obvious impression of a proximal tibia. Refitting of the fossil to the block indicates that roughly 33mm of proximal tibia separates the most proximal break in the *U.W. 88-40* shaft from the most proximal impression made by the tibia in the block of calcified sediment. Articulating *U.W. 88-40* with *U.W. 88-21* (far right) shows that 229 mm of the tibia is present. Therefore, the tibia would have been a minimum of 262 mm. Because it was the anterior portion of the tibia that left the impression in the block, the degree of retroversion would directly impact this estimate of length. Accounting as well for the proximal projection of the tibial spines (using casts of *Australopithecus* proximal tibiae A.L. 129-1, A.L. 288-1, and StW 514 as comparisons), we estimate that the MH4 tibia would have been about 271 mm (ranges independently assessed by 4 co-authors of this paper between 267-275 mm).

Fig. S13. The *Australopithecus sediba* foot and ankle reconstructed in anatomical positioning. On the top are images (top left: lateral; top second to right: posterior) of the conjoined MH2 foot and ankle (*U.W. 88-97, 98, 99*) as they were recovered. As described elsewhere (*1,7*), the bones were medical CT-scanned, digitally segmented, and casts were produced. At the top (second to left and far right), the casts are reconfigured in anatomical position. In posterior view, notice that the heel is in an inverted set and the area of the heel in contact with the ground during heel-strike is exceptionally small. In the bottom images, a chimpanzee (far left) and human (far right) are compared to *Au. sediba* in posterior view. Notice that as in humans, the *Au. sediba* ankle is orthogonal to the substrate; whereas the tibia angles laterally in the chimpanzee. This geometry of the ankle joint is correlated with the bicondylar angle of the knee. In humans (right), the plantar repositioning of the lateral plantar process (arrow) increases the surface area of the heel. The superiorly-positioned lateral plantar process in the *Au. sediba* foot has been discussed elsewhere (*7*). The exceptionally small heel area in contact with the ground would increase the stress associated with heel strike, suggesting that *Au. sediba* may have used a different strategy for dissipating the forces associated with heel strike. We suggest that the heel and lateral midfoot may have simultaneously contacted the ground during bipedal gait, as happens during quadrupedal gait in bonobos (*31*).

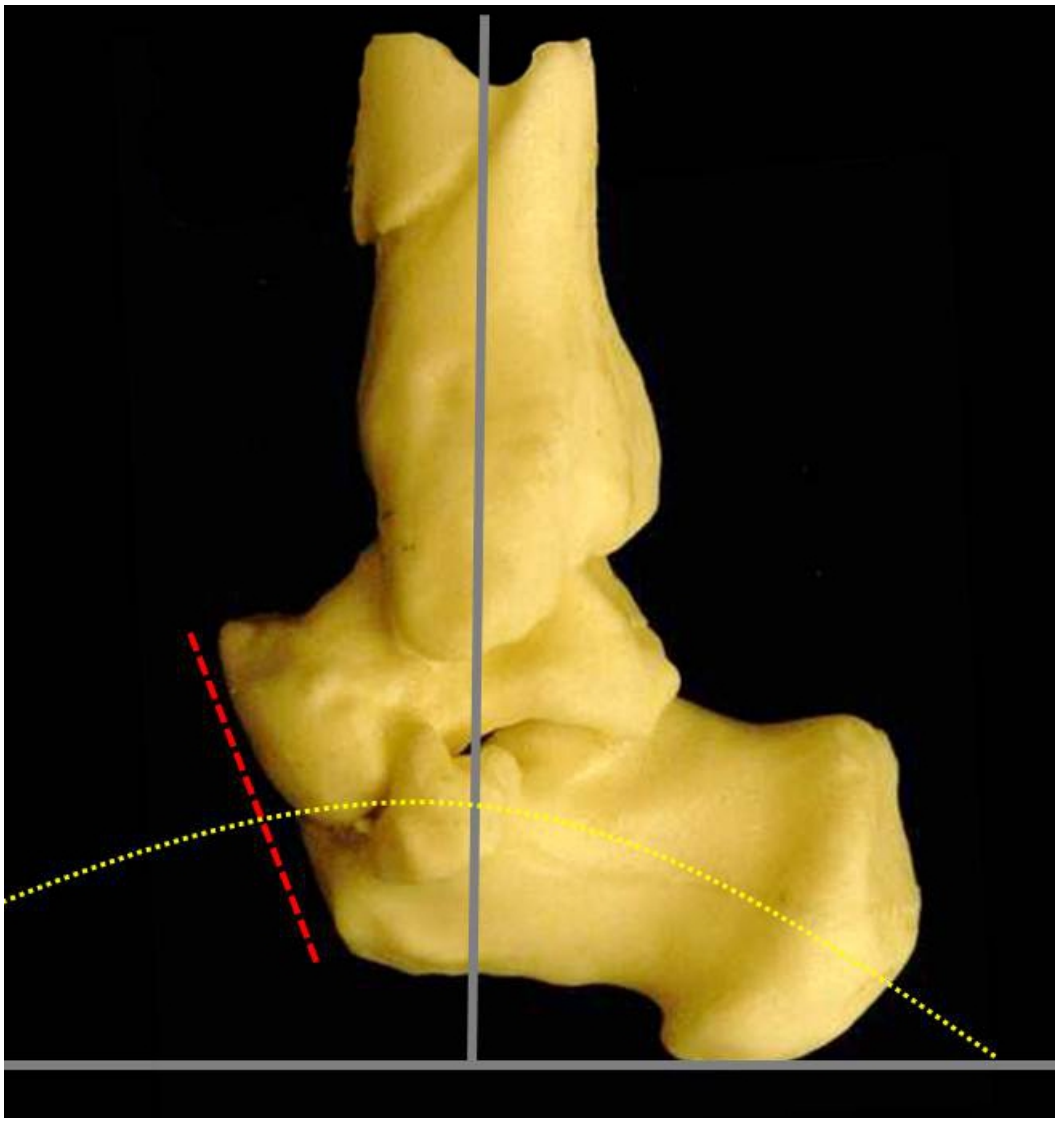

Fig. S14. Casts of the tibia, talus, and calcaneus of *Au. sediba* are shown here, in medial view, in proper anatomical positioning. We previously argued (*7*) that these bones, in isolation, provide evidence for a longitudinal arch. Here, we show that when the tibia is oriented perpendicularly to the ground (gray solid lines), and is centrally positioned on the talus, that the foot is necessarily arched (yellow dotted line). The plantarly angled talar head and calcaneocuboid facet (red dashed line) are instead orthogonal in flat-footed apes, and this angulation is only possible in a foot that has at least a moderate longitudinal arch.

Fig. S15. The MH2 ilium in external perspective (from *9*). The arrow is pointing to the hypertrophied anterior inferior iliac spine. Both the rectus femoris and the iliofemoral ligament originate from this region. We suggest in this paper that hyperpronation in *Au. sediba*, and particularly in MH2, produced excessive strain on the rectus femoris and resulted in this enlarged AIIS.

SM TEXT: Evidence for hyperpronating gait in *Australopithecus sediba*.

The majority of anatomical evidence for a hyperpronating gait in *Australopithecus sediba* comes from the adult female skeleton MH2. This raises the question of whether this particular individual (MH2) walked with hyperpronation, or if her anatomy is indicative of how the entire species walked. It will take the discovery of more fossils from additional individuals to test our hypothesis that the species *Au. sediba* was adapted for moving in this particular manner. However, below we present in more detail the evidence that the gait of MH2 may not have been unusual for her species, and may have typified locomotion in this late australopith.

1. Pronation not only everts the foot, but adducts and plantarflexes the talus on the calcaneus at the subtalar joint. This motion lowers the longitudinal arch and aligns the axes of the transverse tarsal joints (*77*), making the midfoot more mobile during the stance phase of gait. Excessive pronation can therefore result in hypermobility of the midfoot region. We present evidence in this paper that *Au. sediba* had excessive mobility in the sagittal plane of the midfoot region, producing a "midtarsal" break, as evidenced by the convexity of the base of the fourth metatarsal *U.W. 88-22*. However, this metatarsal is not associated with the MH2 skeleton. Instead, *U.W. 88-22* more likely belongs to MH1, given that the distal end presents an epiphyseal surface for the unfused metatarsal head and is consistent with the developmental age of MH1 (*1*). The anatomy of *U.W. 88-22* is unusual for hominins, but is entirely consistent with the hypothesis for how the MH2 individual was moving. It seems logical therefore to suggest that MH1 walked in a kinematically similar way as MH2. The alternative hypothesis would be that the anatomy of the midfoot of *Au. sediba* was more ape-like, since apes also have sagittal plane motion at the tarsometatarsal joint (a midtarsal break) without hyperpronating. The midtarsal break in apes is possible in part because they lack soft tissue structures of the longitudinal arch, like the long plantar ligament, which stiffen the midfoot (*40*). We have presented evidence here and elsewhere (*7*), that *Au. sediba* likely possessed many of the soft-tissue components of the longitudinal arch, including the long plantar ligament. The mobility of the tarsometatarsal joint is therefore best explained by a hyperpronating gait in our opinion. However, we remain open to the possibility that more ape-like mobility at the calcaneocuboid joint, the absence of a plantar aponeurosis, or an ape-like path of the peroneus longus through the midfoot (*32*) could also explain this midfoot hypermobility. Additional pedal fossils, especially a cuboid and medial cuneiform, will help test these hypotheses.
2. The starting point for hypothesizing that *Au. sediba* walked with hyperpronation is the morphology of the calcaneus. An inverted calcaneus possessing a small contact area with the ground (in other words, an ape-like heel) causes the initial contact with the ground to be along the lateral edge of the heel and midfoot (as is found in apes). Contacting the ground along the lateral edge of the foot necessarily creates a pronatory torque. The ape-like anatomy of the MH2 calcaneus, with a small heel, and an elevated lateral plantar process, is unusual for hominins, but it is not unusual for *Au. sediba*. *U.W. 88-113* is a calcaneal apophysis from MH1 that has the same anatomy as the adult calcaneus, with a small, beak-like medial plantar process, and a superiorly positioned lateral plantar process (*7*). This anatomy suggests that both MH1 and MH2 would have walked along the lateral edge of a slightly inverted foot that would have been driven into excessive

pronation by the position of the ground reaction resultant relative to the joints of the foot. There are only two ways in which walking along the lateral edge of an inverted foot would *not* cause hyperpronation at the subtalar, midtarsal, and tarsometatarsal joints. (i) Muscular action of the inverters of the foot (anterior and posterior tibialis, for example) could keep the foot in an inverted set despite the ground reaction forces acting to drive the foot into pronation. (ii) If the position of the center of mass were lateral to the joints of the foot, there would be a counteracting supinatory torque produced during single-legged stance. Chimpanzees, and other apes, shift their center of mass laterally over the stance leg during bipedal gait, since their lesser gluteals do not act as hip abductors, as is the case in humans. However, the ilia of *Au. sediba* are sagittally oriented (*9*), and we interpret this anatomy as being fully consistent with a human-like abductor mechanism at the hip joint during single-legged stance phase. This arrangement would likely keep the center of mass of *Au. sediba* medial to the joints of the foot, and, if anything, exacerbate the pronatory torque around the joints of the foot over much of the first half of stance phase. This extreme pronatory torque could be mitigated by a moderately divergent hallux, which would produce a counter supinatory torque. However, the anatomy of the first pedal ray is currently unknown in *Au. sediba*.

3. Contacting the substrate on an inverted foot (which sets the stage for hyperpronation) was argued in this paper to introduce a shear force across the medial malleolus. The MH2 skeleton (*U.W. 88-97*) possesses a mediolaterally thickened medial malleolus, which would help resist these shear forces and may be an adaptation for loading an inverted foot (*7*). However, while this anatomy is unusual for hominins, it is not unusual for *Au. sediba*. *U.W. 88-21* is a right distal tibia from another adult individual (MH4) and it too possesses a thickened medial malleolus, suggesting that both MH2 and MH4 could resist the high shear forces that result from loading an inverted ankle.
4. Excessive pronation causes internal rotation of the femur and an elevated risk for lateral patellar subluxation (*45, 46*). The elevated lateral lip of the distal femur of MH2 would reduce this risk of patellar dislocation. It has been shown that in humans, the height of the lateral lip is relatively unchanged from birth to adulthood (*17, 18, 78*). The fact that the MH2 distal femur possesses an exceptionally high lateral lip, together with evidence that the relative lateral lip height is the same in newborns as in adults, suggests that the high lateral lip in MH2 is not just a bony adaptation that was developed over the course of MH2's lifetime to counter the tendency of the patella to pull laterally during hyperpronating gait. We regard this as evidence that MH2 was born with a structural solution in anticipation of a functional challenge that would not have been encountered until MH2 started hyperpronating during the course of independent gait. This suggests that *Au. sediba*, and not just MH2, walked in this manner.

References and Notes

1. L. R. Berger *et al*., *Australopithecus sediba*: A new species of *Homo*-like australopith from South Africa. *Science* **328**, 195 (2010). doi:10.1126/science.1184944 Medline

2. R. Pickering *et al*., *Australopithecus sediba* at 1.977 Ma and implications for the origins of the genus *Homo*. *Science* **333**, 1421 (2011). doi:10.1126/science.1203697 Medline

3. T. L. Kivell, J. M. Kibii, S. E. Churchill, P. Schmid, L. R. Berger, *Australopithecus sediba* hand demonstrates mosaic evolution of locomotor and manipulative abilities. *Science* **333**, 1411 (2011). doi:10.1126/science.1202625 Medline

4. S. E. Churchill *et al*., The upper limb of *Australopithecus sediba*. *Science* **340**, 1233477 (2013).

5. P. Schmid *et al*., Mosaic morphology in the thorax of *Australopithecus sediba*. *Science* **340**, 1234598 (2013).

6. S. Williams *et al*., The vertebral column of *Australopithecus sediba*. *Science* **340**, 1232996 (2013).

7. B. Zipfel *et al*., The foot and ankle of *Australopithecus sediba*. *Science* **333**, 1417 (2011). doi:10.1126/science.1202703 Medline

8. K. J. Carlson *et al*., The endocast of MH1, *Australopithecus sediba*. *Science* **333**, 1402 (2011). doi:10.1126/science.1203922 Medline

9. J. M. Kibii *et al*., A partial pelvis of *Australopithecus sediba*. *Science* **333**, 1407 (2011). doi:10.1126/science.1202521 Medline

10. D. J. de Ruiter *et al*., Mandibular remains support taxonomic validity of *Australopithecus sediba*. *Science* **340**, 1232997 (2013).

11. J. D. Irish, D. Guatelli-Steinberg, S. S. Legge, L. R. Berger, D. J. de Ruiter, Dental morphology and the phylogenetic “place” of *Australopithecus sediba*. *Science* **340**, 1233062 (2013).

12. W. E. H. Harcourt-Smith, L. C. Aiello, Fossils, feet and the evolution of human bipedal locomotion. *J. Anat.* **204**, 403 (2004). doi:10.1111/j.0021-8782.2004.00296.x Medline

13. Y. Haile-Selassie *et al*., A new hominin foot from Ethiopia shows multiple Pliocene bipedal adaptations. *Nature* **483**, 565 (2012). doi:10.1038/nature10922 Medline

14. Methods and background are available as supplementary materials on *Science* Online.

15. C. O. Lovejoy, R. S. Meindl, J. C. Ohman, K. G. Heiple, T. D. White, The Maka femur and its bearing on the antiquity of human walking: Applying contemporary concepts of morphogenesis to the human fossil record. *Am. J. Phys. Anthropol.* **119**, 97 (2002). doi:10.1002/ajpa.10111 Medline

16. B. Asfaw, Proximal femur articulation in Pliocene hominids. *Am. J. Phys. Anthropol.* **68**, 535 (1985). doi:10.1002/ajpa.1330680409 Medline

17. C. Tardieu, Development of the human hind limb and its importance for the evolution of bipedalism. *Evol. Anthropol.* **19**, 174 (2010). doi:10.1002/evan.20276

18. C. O. Lovejoy, The natural history of human gait and posture. Part 3. The knee. *Gait Posture* **25**, 325 (2007). doi:10.1016/j.gaitpost.2006.05.001 Medline

19. C. Tardieu *et al*., Relationship between formation of the femoral bicondylar angle and trochlear shape: Independence of diaphyseal and epiphyseal growth. *Am. J. Phys. Anthropol.* **130**, 491 (2006). doi:10.1002/ajpa.20373 Medline

20. J. A. Wanner, Variations in the anterior patellar groove of the human femur. *Am. J. Phys. Anthropol.* **47**, 99 (1977). doi:10.1002/ajpa.1330470117 Medline

21. W. E. Clark, Observations on the anatomy of the fossil Australopithecinae. *J. Anat.* **81**, 300 (1947). Medline

22. K. G. Heiple, C. O. Lovejoy, The distal femoral anatomy of *Australopithecus*. *Am. J. Phys. Anthropol.* **35**, 75 (1971). doi:10.1002/ajpa.1330350109 Medline

23. C. Tardieu, Morpho-functional analysis of the articular surfaces of the knee-joint in primates, in *Primate Evolutionary Biology*, A. B. Chiarelli, R. S. Corruccini, Eds. (Springer-Verlag, New York, 1981), pp. 68–80.

24. L. C. Aiello, M. C. Dean, *An Introduction to Human Evolutionary Anatomy* (Academic Press, London, 1990).

25. J. M. Organ, C. V. Ward, Contours of the hominoid lateral tibial condyle with implications for *Australopithecus*. *J. Hum. Evol.* **51**, 113 (2006). doi:10.1016/j.jhevol.2006.01.007 Medline

26. B. Senut, C. Tardieu, Functional aspects of Plio-Pleistocene hominid limb bones: Implications for taxonomy and phylogeny, in *Ancestors: The Hard Evidence*, E. Delson, Ed. (Alan R. Liss, New York, 1985), pp. 193–201.

27. J. Dugan, T. W. Holliday, Utility of the lateral meniscal notch in distinguishing hominin taxa. *J. Hum. Evol.* **57**, 773 (2009). doi:10.1016/j.jhevol.2009.07.006 Medline

28. Pronation of the foot is a triplanar motion (eversion, abduction, and dorsiflexion occurring simultaneously) and is a normal function of bipedal foot mechanics in order to absorb ground reaction forces and accommodate uneven substrates. It converts the foot from a rigid structure at heel strike to a more mobile one at midstance. Hyperpronation is poorly defined in a clinical sense, because there is no distinct cutoff between those that excessively pronate and those who do not. However, here we define it as continued pronation into the part of stance phase when the foot should be resupinating (usually at the later part of midstance and during the entire propulsive phase). Extended (timing-wise) pronation is caused both by the magnitude of pronation (in degrees) that occurs as a result of the large pronatory torque generated by contacting the ground on a varus heel and forefoot, and the timing of foot motion. Because of the excessive motion occurring at the subtalar, midtarsal, and tarsometatarsal joints, the foot fails to resupinate at late stance and pushoff.

29. D. L. Gebo, Plantigrady and foot adaptation in African apes: Implications for hominid origins. *Am. J. Phys. Anthropol.* **89**, 29 (1992). doi:10.1002/ajpa.1330890105 Medline

30. H. Elftman, J. Manter, Chimpanzee and human feet in bipedal walking. *Am. J. Phys. Anthropol.* **20**, 69 (1935). doi:10.1002/ajpa.1330200109

31. E. Vereecke, K. D'Août, D. De Clercq, L. Van Elsacker, P. Aerts, Dynamic plantar pressure distribution during terrestrial locomotion of bonobos (*Pan paniscus*). *Am. J. Phys. Anthropol.* **120**, 373 (2003). doi:10.1002/ajpa.10163 Medline

32. C. O. Lovejoy, B. Latimer, G. Suwa, B. Asfaw, T. D. White, Combining prehension and propulsion: The foot of *Ardipithecus ramidus. Science* **326**, 72e1-e8 (2009).

33. K. D. Gross *et al*., Varus foot alignment and hip conditions in older adults. *Arthritis Rheum.* **56**, 2993 (2007). doi:10.1002/art.22850 Medline

34. K. G. Holt, J. Hamill, Running injuries and treatment: A dynamic approach, in *Rehabilitation of the Foot and Ankle*, G. J. Sammarco, Ed. (Mosby, St. Louis, MO, 1995), pp. 241–258.

35. L. Wong, A. Hunt, J. Burns, J. Crosbie, Effect of foot morphology on center-of-pressure excursion during barefoot walking. *J. Am. Podiatr. Med. Assoc.* **98**, 112 (2008). Medline

36. T. C. Michaud, The foot: hyperpronation and hypopronation, in *Functional Soft-Tissue Examination and Treatment by Manual Methods*, W. I. Hammer, Ed. (Jones and Bartlett, Sudbury, MA, 2005), pp. 399–426.

37. K. A. Kirby, Subtalar joint axis location and rotational equilibrium theory of foot function. *J. Am. Podiatr. Med. Assoc.* **91**, 465 (2001). Medline

38. M. B. Bennett, R. F. Ker, The mechanical properties of the human subcalcaneal fat pad in compression. *J. Anat.* **171**, 131 (1990). Medline

39. T. J. Ouzounian, M. J. Shereff, In vitro determination of midfoot motion. *Foot Ankle* **10**, 140 (1989). doi:10.1177/107110078901000305 Medline

40. J. M. DeSilva, Revisiting the "midtarsal break". *Am. J. Phys. Anthropol.* **141**, 245 (2010). Medline

41. C. V. Ward, W. H. Kimbel, D. C. Johanson, Complete fourth metatarsal and arches in the foot of *Australopithecus afarensis*. *Science* **331**, 750 (2011). doi:10.1126/science.1201463 Medline

42. D. Tiberio, The effect of excessive subtalar joint pronation on patellofemoral mechanics: A theoretical model. *J. Orthop. Sports Phys. Ther.* **9**, 160 (1987). Medline

43. S. Khamis, Z. Yizhar, Effect of feet hyperpronation on pelvic alignment in a standing position. *Gait Posture* **25**, 127 (2007). doi:10.1016/j.gaitpost.2006.02.005 Medline

44. C. M. Powers, R. Maffucci, S. Hampton, Rearfoot posture in subjects with patellofemoral pain. *J. Orthop. Sports Phys. Ther.* **22**, 155 (1995). Medline

45. B. A. Rothbart, L. Estabrook, Excessive pronation: A major biomechanical determinant in the development of chondromalacia and pelvic lists. *J. Manipulative Physiol. Ther.* **11**, 373 (1988). Medline

46. J. J. Eng, M. R. Pierrynowski, Evaluation of soft foot orthotics in the treatment of patellofemoral pain syndrome. *Phys. Ther.* **73**, 62, discussion 68 (1993). Medline

47. M. R. Bennett *et al*., Early hominin foot morphology based on 1.5-million-year-old footprints from Ileret, Kenya. *Science* **323**, 1197 (2009). doi:10.1126/science.1168132 Medline

48. R. H. Crompton *et al*., Human-like external function of the foot, and fully upright gait, confirmed in the 3.66 million year old Laetoli hominin footprints by topographic statistics, experimental footprint-formation and computer simulation. *J. R. Soc. Interface* **9**, 707 (2012). doi:10.1098/rsif.2011.0258 Medline

49. B. Latimer, C. O. Lovejoy, Hallucal tarsometatarsal joint in *Australopithecus afarensis*. *Am. J. Phys. Anthropol.* **82**, 125 (1990). doi:10.1002/ajpa.1330820202 Medline

50. H. M. McHenry, L. R. Berger, Body proportions of *Australopithecus afarensis* and *A. africanus* and the origin of the genus *Homo*. *J. Hum. Evol.* **35**, 1 (1998). doi:10.1006/jhev.1997.0197 Medline

51. D. J. Green, A. D. Gordon, B. G. Richmond, Limb-size proportions in *Australopithecus afarensis* and *Australopithecus africanus*. *J. Hum. Evol.* **52**, 187 (2007). doi:10.1016/j.jhevol.2006.09.001 Medline

52. J. T. Stern Jr., R. L. Susman, The locomotor anatomy of *Australopithecus afarensis*. *Am. J. Phys. Anthropol.* **60**, 279 (1983). doi:10.1002/ajpa.1330600302 Medline

53. R. Wunderlich, thesis, State University of New York at Stony Brook, Stony Brook, NY (1999).

54. W. S. Rasband, J. Image, U.S. National Institutes of Health, Bethesda, MD, 1997–2012; http://imagej.nih.gov/ij/.

55. K. E. Reed, J. W. Kitching, F. E. Grine, W. L. Jungers, L. Sokoloff, Proximal femur of *Australopithecus africanus* from Member 4, Makapansgat, South Africa. *Am. J. Phys. Anthropol.* **92**, 1 (1993). doi:10.1002/ajpa.1330920102 Medline

56. C. O. Lovejoy, Biomechanical perspectives on the lower limb of early hominids, in *Primate Functional Morphology and Evolution*, R. Tuttle, Ed. (Mouton, The Hague, Netherlands, 1975), pp. 291–326.

57. C. O. Lovejoy, D. C. Johanson, Y. Coppens, Hominid lower limb bones recovered from the Hadar formation: 1974-1977 collections. *Am. J. Phys. Anthropol.* **57**, 679 (1982). doi:10.1002/ajpa.1330570411

58. D. C. Johanson *et al*., Morphology of the Pliocene partial hominid skeleton (A.L. 288-1) from the Hadar formation, Ethiopia. *Am. J. Phys. Anthropol.* **57**, 403 (1982). doi:10.1002/ajpa.1330570403

59. M. Pickford, B. Senut, D. Gommery, J. Treil, Bipedalism in *Orrorin tugenensis* revealed by its femora. *C. R. Palevol* **1**, 191 (2002). doi:10.1016/S1631-0683(02)00028-3

60. C. V. Ward, W. H. Kimbel, E. H. Harmon, D. C. Johanson, New postcranial fossils of *Australopithecus afarensis* from Hadar, Ethiopia (1990-2007). *J. Hum. Evol.* **63**, 1 (2012). doi:10.1016/j.jhevol.2011.11.012 Medline

61. D. DeGusta, thesis, University of California at Berkeley, Berkeley, CA (2004).

62. T. C. Partridge, D. E. Granger, M. W. Caffee, R. J. Clarke, Lower Pliocene hominid remains from Sterkfontein. *Science* **300**, 607 (2003). doi:10.1126/science.1081651 Medline

63. A. C. Walker, New *Australopithecus* femora from East Rudolf, Kenya. *J. Hum. Evol.* **2**, 545 (1973). doi:10.1016/0047-2484(73)90132-2

64. T. R. Pickering *et al.*, New hominid fossils from Member 1 of the Swartkrans formation, South Africa. *J. Hum. Evol.* **62**, 618 (2012). doi:10.1016/j.jhevol.2012.02.003 Medline

65. M. H. Day, R. E. F. Leakey, A. C. Walker, B. A. Wood, New hominids from East Turkana, Kenya. *Am. J. Phys. Anthropol.* **45**, 369 (1976). doi:10.1002/ajpa.1330450304 Medline

66. M. H. Day, R. E. F. Leakey, A. C. Walker, B. A. Wood, New hominids from East Rudolf, Kenya, I. *Am. J. Phys. Anthropol.* **42**, 461 (1975). doi:10.1002/ajpa.1330420314 Medline

67. D. C. Johanson *et al.*, New partial skeleton of *Homo habilis* from Olduvai Gorge, Tanzania. *Nature* **327**, 205 (1987). doi:10.1038/327205a0 Medline

68. D. Lordkipanidze *et al.*, Postcranial evidence from early *Homo* from Dmanisi, Georgia. *Nature* **449**, 305 (2007). doi:10.1038/nature06134 Medline

69. A. C. Walker, R. E. F. Leakey, The postcranial bones, in *The Nariokotome* Homo erectus *skeleton*, A. C. Walker, R. E. F. Leakey, Eds. (Harvard Univ. Press, Cambridge, MA, 1993), pp. 95–160.

70. W. H. Gilbert, Daka member hominid postcranial remains, in Homo erectus. *Pleistocene Evidence from the Middle Awash, Ethiopia*, W. H. Gilbert, B. Asfaw, Eds. (Univ. of California Press, Berkeley, CA, 2008), pp. 373–396.

71. M. H. Day, R. E. F. Leakey, New evidence of the genus *Homo* from East Rudolf, Kenya (III). *Am. J. Phys. Anthropol.* **41**, 367 (1974). doi:10.1002/ajpa.1330410304

72. F. E. Grine, W. L. Jungers, P. V. Tobias, O. M. Pearson, Fossil *Homo* femur from Berg Aukas, northern Namibia. *Am. J. Phys. Anthropol.* **97**, 151 (1995). doi:10.1002/ajpa.1330970207 Medline

73. W. L. Jungers *et al.*, Descriptions of the lower limb skeleton of *Homo floresiensis*. *J. Hum. Evol.* **57**, 538 (2009). doi:10.1016/j.jhevol.2008.08.014 Medline

74. R. E. F. Leakey, A. C. Walker, Further hominids from the Plio-Pleistocene of Koobi Fora, Kenya. *Am. J. Phys. Anthropol.* **67**, 135 (1985). doi:10.1002/ajpa.1330670209 Medline

75. W. M. Bass, *Human Osteology. A Laboratory and Field Manual* (Missouri Archaeology Society, Columbia, MO, 1995).

76. R. L. Susman, J. T. Stern, Functional morphology of *Homo habilis*. *Science* **217**, 931 (1982). doi:10.1126/science.217.4563.931 Medline

77. H. Elftman, The transverse tarsal joint and its control. *Clin. Orthop.* **16**, 41 (1960). Medline

78. Y. Glard *et al*., An anatomical and biometrical study of the femoral trochlear groove in the human fetus. *J. Anat.* **206**, 411 (2005). doi:10.1111/j.1469-7580.2005.00400.x Medline